frontiers | Frontiers in Earth Science

TYPE Original Research
PUBLISHED 28 June 2023
DOI 10.3389/feart.2023.1177240

OPEN ACCESS

EDITED BY
Vahid Tavakoli,
University of Tehran, Iran

REVIEWED BY
Mastaneh Liseroudi,
Department of Natural Resources, Canada
Shailesh Agrawal,
Birbal Sahni Institute of Palaeosciences (BSIP), India

*CORRESPONDENCE
Ming Ma,
mam@lzb.ac.cn

RECEIVED 01 March 2023
ACCEPTED 16 June 2023
PUBLISHED 28 June 2023

CITATION
Ma M, Lei C and Rahman MJJ (2023), Paleoenvironmental reconstruction of the Eocene sediments in the Baiyun sag of the Pearl River Mouth Basin. *Front. Earth Sci.* 11:1177240. doi: 10.3389/feart.2023.1177240

Paleoenvironmental reconstruction of the Eocene sediments in the Baiyun sag of the Pearl River Mouth Basin

Ming Ma[1,2,3]*, Chao Lei[2,4] and M. Julleh Jalalur Rahman[5]

[1]Northwest Institute of Eco-Environment and Resources, Chinese Academy of Sciences, Lanzhou, China, [2]Hubei Key Laboratory of Marine Geological Resources, China University of Geosciences, Wuhan, China, [3]Key Laboratory of Petroleum Resources, Lanzhou, China, [4]College of Marine Science and Technology, China University of Geosciences, Wuhan, China, [5]Department of Geological Sciences, Jahangirnagar University, Dhaka, Bangladesh

The Baiyun sag of the Pearl River Mouth Basin has become a focus for deepwater exploration with the highest hydrocarbon potential in northern South China Sea. The Eocene organic-rich mudstones are the main source rocks in the Baiyun sag, and the evolution of their depositional environment remains unclear. Based on the core and geochemical data, we investigated the depositional environments of the Eocene Wenchang and Enping sediments in the Baiyuan sag and revealed the sedimentary environment influences on the formation of the source rocks in the study area. The results indicate that the sediments of the Wenchang and Enping formations were deposited in dysoxic to oxic environments. Moreover, according to the concentrations of salinity-sensitive trace elements, and $\delta^{13}C$ (-10.9‰ to -7.2‰, average -8.58‰) and $\delta^{18}O$ (-18.4‰ to -14.5‰, average -17.1‰) values of carbonate cement in the sandstone samples, the Wenchang and Enping formations were in fresh water to brackish water conditions during their deposition, with increasing salinity from bottom to top, which suggests that the two formations were mainly deposited in lacustrine environment and the Enping formation experienced a relatively extensive lake transgression. The vertical variations of geochemical characteristics suggest that the Wenchang and Enping formations were deposited under a semi-arid/warm condition and all Eocene sediments experienced mild to moderate chemical weathering, relatively large detrital input and stable paleowater depth. Both primary productivity and preservation conditions played essential roles in controlling the enrichment of organic matters in the Baiyun sag, and the preservation conditions resulted from the restricted water setting. The present work provide a comprehensive analysis of depositional environments based on the abundance of high-resolution geochemical data. The results obtained reveal the dominated factors controlling organic matter enrichment in the Baiyun Sag of the Pearl River Mouth Basin. Those findings are not only significant for understanding the region's paleogeography, but also provide guidance for future profitable oil and gas exploration in the northern South China Sea and other similar areas.

KEYWORDS

paleoenvironment, paleoclimate, paleoweathering, paleoproductivity, Eocene, Baiyun sag, Pearl River Mouth Basin

1 Introduction

The South China Sea (SCS) is the largest and deepest marginal sea in the western Pacific Ocean (Sun et al., 2012). At the northern continental margin of SCS, there are multiple extensional basins, including the Pearl River Mouth Basin (PRMB) (Xie et al., 2014). The Baiyun sag in the center of PRMB is a key exploration area in the basin. Over the past three decades, several significant gas fields like LW3-1 were discovered in the Baiyun sag, confirming it as the most promising target of deepwater oil exploration in northern SCS (Mi et al., 2018; Xu et al., 2021). Many researchers have studied the source rocks in the Baiyun sag from the perspective of provenance, geological structure, sequence stratigraphy, depositional system, geochemical characteristics, and pressure distribution/evolution (Xie et al., 2014; Shao et al., 2016; Chen et al., 2018; He et al., 2018; Kong et al., 2018; Lin et al., 2018; Zhao et al., 2018; Fu et al., 2019; Ma et al., 2019; He et al., 2020; Yuan et al., 2021; Jiang et al., 2022). The study on depositional system mainly focuses on the provenance and sequence stratigraphy of medium-scale and large-scale progradational braided deltas, beach bars, fan deltas and deep-water fan system (Pang et al., 2007; Lin et al., 2018; Ma et al., 2019; Wang et al., 2019; Zeng et al., 2019). At present, the depositional environment during the Enping Formation of the Baiyun sag in the PRMB remains a topic of debate: 1) A restricted marine depositional environment for the Baiyun and Liwan sags during the Enping Formation (Miao et al., 2013); 2) The Baiyun sag was a relatively closed terestrial rifted lake basin with fresh water environment during this time (Zeng et al., 2019; Shi et al., 2020). The reason for the lack of study and controversial research on the sedimentary environment is the limited availability of deep water samples. In this study, we investigated the depositional environment using elemental geochemistry of the sediments from the Eocene Wenchang and Enping formations in the Baiyun sag, with an aim to provide valuable reference to the prediction of high-quality source rocks (terrestrial organic matter and mixed organic matter) and thus support future petroleum exploration and development in the northern SCS.

High-quality source rocks provide materials for the formation of medium–large reservoirs and also record the evolution of paleoenvironment (Zhao et al., 2021). Paleoenvironment can be determined by analysis of lithofacies and elemental geochemistry of the source rocks (Vincent et al., 2006; Ma et al., 2016). The paleoenvironment can be accurately and efficiently reconstructed from major elements, trace elements, and their ratios (Moradi et al., 2016). Many scholars used the concentrations and/or ratios of elements to investigate the paleoredox (U, Mo, Ni, V, Cr, Co, Fe, Cu, Zn and Re), paleosalinity (Sr, Ba, B and Ga), paleoclimate (C-value), paleoweathering (chemical index of alteration, CIA; chemical index of weathering, CIW; plagioclase index of alteration, PIA) and paleoproductivity (Ba and P) (Nesbitt and Young, 1982; Cao et al., 2012; Algeo and Li, 2020; Wei and Algeo, 2020a; Bennett et al., 2020; Liu et al., 2020). Clearly, elemental geochemistry can be embraced to determine the depositional conditions and organic matter enrichment of source rocks. In addition, paleoclimate and paleoredox are the environmental factors controlling the distribution of rare Earth element (REE) in fine-grained sediments (Tanaka et al., 2007; Zanin et al., 2010; Bai et al., 2015; Wang Z. et al., 2018).

In this paper, the elemental geochemistry of the Eocene Wenchang and Enping sediments in the Baiyun sag is analyzed by X-ray diffraction (XRD) and inductively coupled plasma-mass spectrometry (ICP-MS). On this basis, the paleoredox, paleosalinity, paleoclimate, paleoweathering, and paleoproductivity are discussed, and the principal mechanisms of organic matter enrichment and the depositional environment are discussed.

2 Geological setting

PRMB is the largest basin in the continental margin of northern South China Sea. It was formed by rifting of the South China Block during the Paleogene and subsequent subsidence during the Neogene. The Baiyun sag is located in the deepwater area of the Zhu II Depression of PRMB. It is adjacent to the Panyu Uplift to the north, the Dongsha Uplift to the northeast, the South Uplift to the south, and the Yunkai Low Uplift to the west (Figure 1) (Ma et al., 2019). As the largest and deepest sag in the basin, the Baiyun sag covers an area of over 20,000 km^2, with a water depth of 200–3000 m (Chen et al., 2015).

The Baiyun sag experienced two major tectonic stages during the Cenozoic: rifting in the Eocene and post-rifting in the early Oligocene to Quaternary (Figure 2) (Jiang et al., 2022). The Eocene strata comprise, from bottom to top, Wenchang (E_2w) and Enping (E_2e) (Figure 2) (He et al., 2018; Kong et al., 2018). During the deposition of the lower and middle members of the Enping Formation, a number of small-to medium-scale braided deltas, fan deltas, and beach bars depositd in the Baiyun sag, however, the sediments deposited in three stages large-scale progradational braided delta during the upper Enping Formation in this area (Zeng et al., 2019). The sediments from the Eocene Wenchang and Enping formations in the Baiyun sag mainly derived from felsic source rock (Ma et al., 2019). The provenance of the Wenchang Formation were mainly provided by the intrabasinal uplift regions (Ma et al., 2019), Dong River and Bei River transported sediments into the Baiyun Sag during the upper Enping Formation (Ma et al., 2019; Wang et al., 2019; Zeng et al., 2019).

3 Samples and methods

3.1 Samples

A total of 14 cutting samples were collected from Wenchang and Enping formations of wells PY27, PY33, BY13, LH29, and LW21 (Table 1 and Table 2). The samples were washed with distilled water to remove possible contaminations and then air-dried. The mudstone samples were crushed to 200 mesh powder by using a mill with tungsten carbide rolls; a part of powder was dried in an oven, weighed and then used for testing the major and trace elements. Geochemical data of other samples are cited from Li et al. (2020). For the data in the figures of this study, the samples of Wenchang Formation are in green colour and Enping Formation are in blue colour.

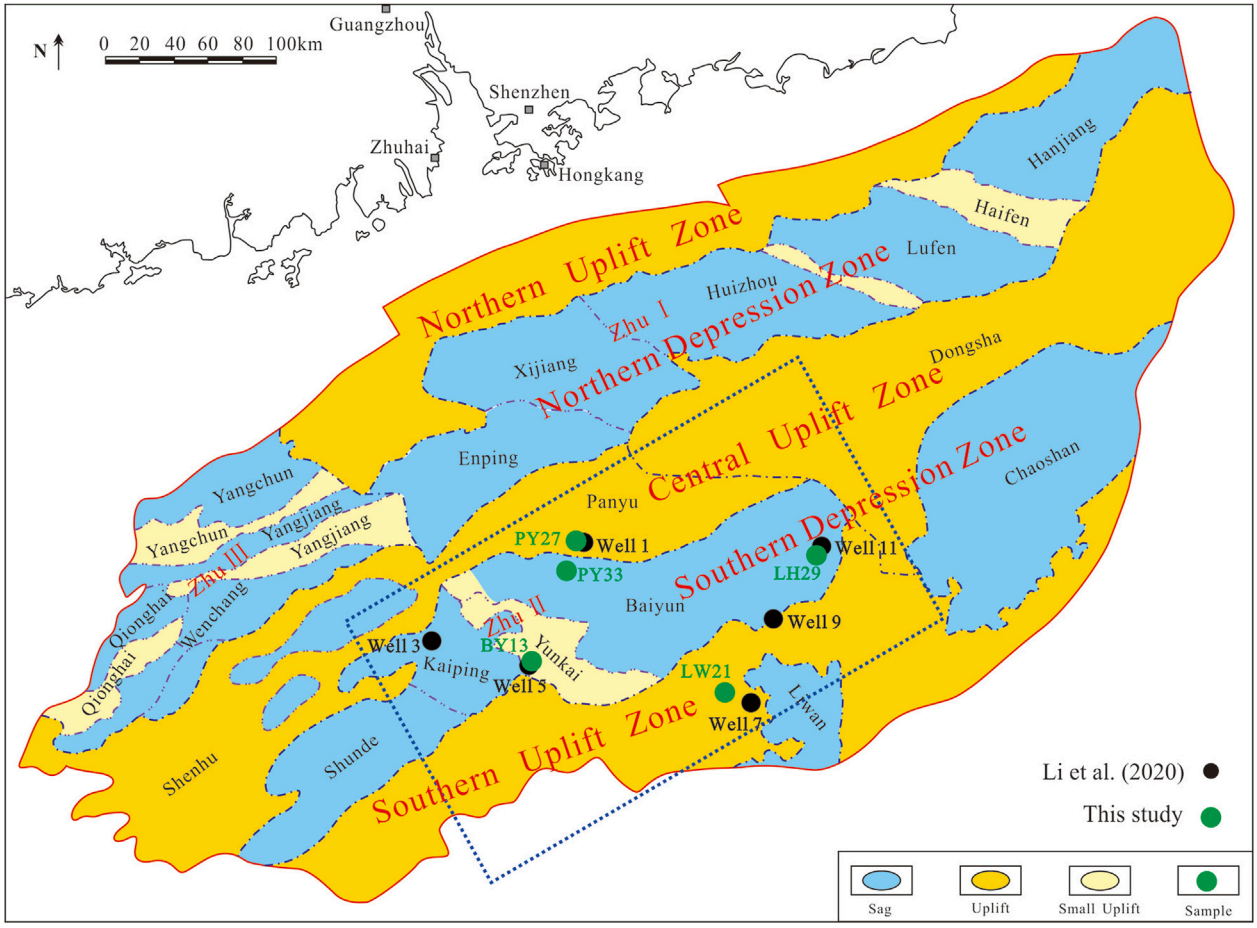

FIGURE 1
Tectonic units of the Pearl River Mouth Basin, and the sampling locations in the Baiyun sag (modified from Zhu & Mi, 2010).

3.2 Methods

Major elements were determined using a fully automated sequential wavelength dispersive X-ray fluorescence spectrometer (AXIOS, PANalytical B.V., Netherlands), at the Key Laboratory of Desert and Desertification, Northwest Institute of Eco-Environment and Resources, Chinese Academy of Sciences (CAS), according to the procedure provided by He et al. (2016). First, 4 g powdered samples were weighed and pressed into a 32-mm-diameter pellet at 30-t pressure. Then, the pellet was stored in desiccator to be analyzed by using a Super Sharp Tube. The estimated accuracy of analysis is >1%.

Trace elements and rare Earth elements (REEs) were determined using ICP-MS (Thermo-elemental, USA) at the Key Laboratory of Tibetan Environment Changes and Land Surface Process, CAS, according to the procedure provided by Ma et al. (2019). The samples were completely digested in pressurized acid using a mixture of HNO_3 and HF. The minimum detection limit of the instrument is less than 1 ppb. The relative error is ±6%. The REEs were normalized to chondrite. The Eu/Eu* anomaly was determined by $\delta Eu=Eu/Eu^*=2\times Eu_N/(Sm_N+Gd_N)$. The Ce/Ce* anomaly was determined by $\delta Ce=Ce/Ce^*=2\times Ce_N/(La_N+Pr_N)$ (Taylor and McLennan, 1985; Ma et al., 2017).

Element enrichment factors (EFs) were calculated according to $X_{EF}=[(X/Al)_{sample}/(X/Al)_{PAAS}]$, where X and Al represent weight percent of elements X and Al, and the subscripts of sample and PAAS denote the sample under study and the Post-Archean Australian Shale (PAAS) standard (Taylor and McLennan, 1985), respectively.

The carbon and oxygen isotope ($\delta^{13}C$ and $\delta^{18}O$) compositions of carbonate cements of sandstone samples were analyzed using a Thermo Finnigan MAT252 mass spectrometer at the Key Laboratory of Petroleum Resources, Gansu Province. The samples were then allowed to react with 100% orthophosphate at a temperature of 90 °C, and then the CO_2 generated from the samples was collected, dried and purified. The values of the carbon and oxygen isotopes analyses were reported relative to the Pee Dee Belemnite (PDB) standard. Isotopic results of the samples are presented in the usual δ notation as the per mil (‰), $\delta=(R_{sample}/R_{standard}-1)\times1000‰$, where R is either the isotopic carbon or oxygen ratio, ($^{13}C/^{12}C$) or ($^{18}O/^{16}O$), respectively.

4 Results

4.1 Major elements

The major element contents are listed in Table 1 and the Supplementary Data from Li et al. (2020). The studied samples

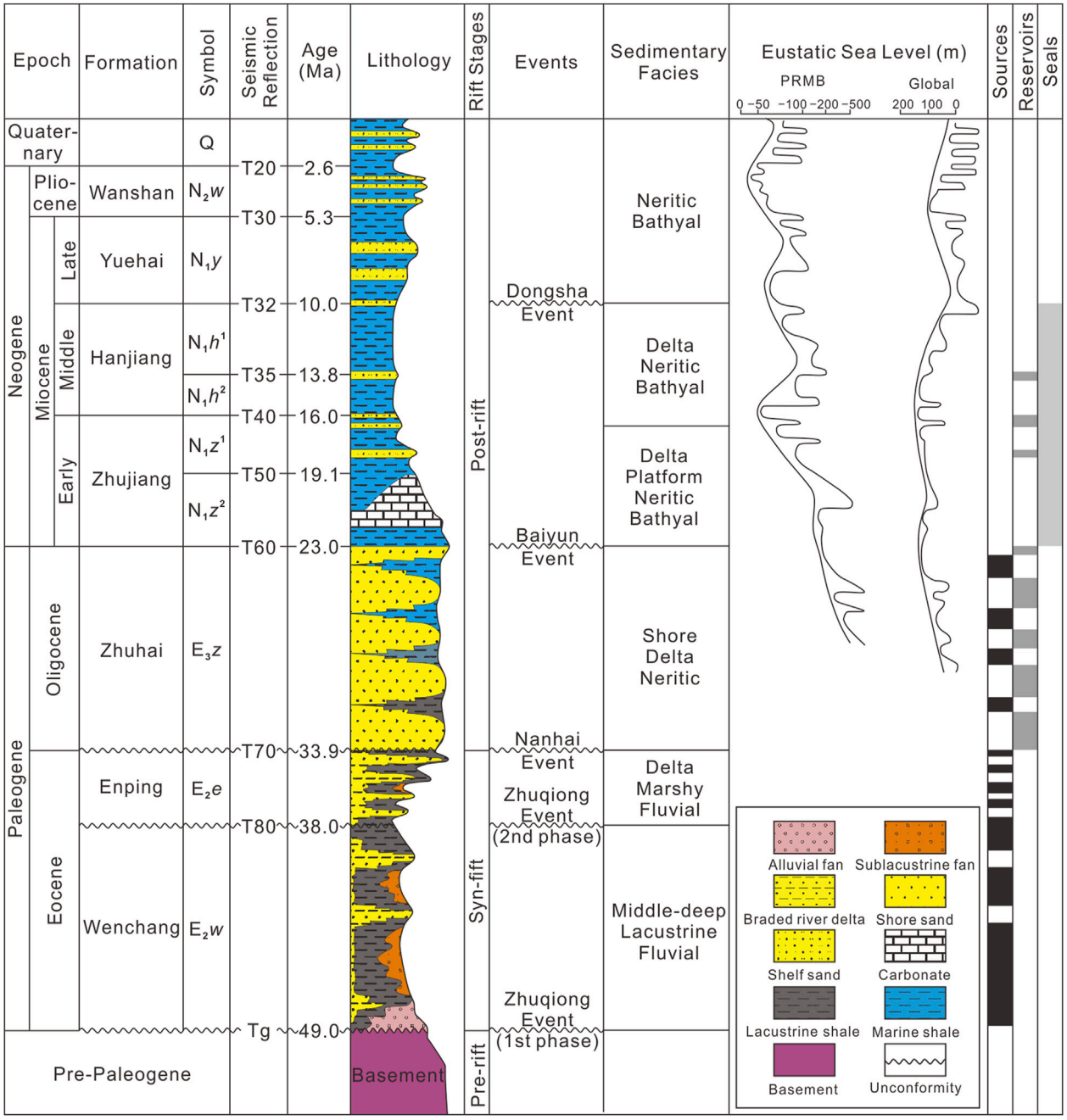

FIGURE 2
Chronology and lithostratigraphy in the Pearl River Mouth Basin. (modified after Kong et al., 2018).

are found with different contents of major elements. The SiO_2 and Al_2O_3 contents are high, being 45.1%–84.99% (avg. 63.01) and 4.34%–24.13% (avg. 16.94), respectively, which may be attributed to the large amount of detrital quartz and clay minerals. The total iron ($Fe_2O_3^T$) content ranges from 1.02% to 23.49% (avg. 5.51), which may relate to the abundance of iron oxide heavy minerals and partly to Fe-containing clay minerals. The MgO and CaO contents show wide ranges, with the former related to the presence of dolomitic materials (mainly ferrodolomite), and the latter mainly attributable to carbonate cement, rock fragments and diagenesis of plagioclase. Almost all samples exhibit much more K_2O than Na_2O, reflecting probably the relative abundance of potassium feldspar. On the log (SiO_2/Al_2O_3) *versus* log (Na_2O/K_2O) diagram (Pettijohn et al., 1972, 1987) (Figure 3A), the samples are mostly plotted in the greywacke, litharenite and arkose areas, and a few in the subarkose area. On the log (SiO_2/Al_2O_3) *versus* log (Fe_2O_3/K_2O) diagram (Herron, 1988) (Figure 3B), most of the samples are tightly clustered in the shale and wacke areas, with a low SiO_2/Al_2O_3, while the other samples are plotted in the Fe-shale, Fe-sand, litharenite, arkose, sublitharenite and subarkose areas. According

10.3389/feart.2023.1177240

TABLE 1 Major element compositions of the Eocene mudstones from the well of PY27, PY33, BY13, LH29, and LW21 in the Baiyun sag.

Well name	PY27	PY33	PY33	PY33	BY13	LH29	LH29	LW21	LW21	LW21	LW21	LW21	LW21
Formation	Enping	Enping	Enping	Enping	Enping	Enping	Enping	Enping	Enping	Wenchang	Wenchang	Wenchang	Wenchang
Depth	4628.6 m	4293.2 m	4295 m	5091 m	2653 m	3110–3119 m	3140–3149 m	3586–3589 m	3646–3649 m	3667–3669 m	3763–3766 m	3865–3868 m	3949–3952 m	4048–4050 m
SiO_2	63.36	67.22	63.7	61.1	59.41	63.13	59.21	64.79	67.25	63.64	61.79	59.79	60.58	62.68
TiO_2	0.71	0.71	0.83	0.72	0.51	0.59	0.70	0.56	0.50	0.58	0.61	0.74	0.62	0.51
Al_2O_3	23.17	21.63	24.13	21.41	22.2	14.71	17.04	19.23	19.19	20.84	20.08	19.89	20.51	20.14
Fe_2O_3	2.01	3.81	2.62	3.85	5.45	4.92	5.78	5.46	4.8	5.64	6.71	6.71	6.57	5.72
MnO	0.0002	0.0003	0.0002	0.0003	0.0005	0.0006	0.0006	0.0006	0.0004	0.0007	0.0010	0.0009	0.0006	0.0006
MgO	1.37	1.41	1.63	2.8	2.65	1.96	2.26	1.7	1.51	1.92	2.8	2.67	2.83	2.4
CaO	0.26	0.26	0.22	0.24	0.77	5.94	5.22	3.24	2.4	1.15	2.57	1.88	1	1.87
Na_2O	0.35	0.34	0.35	0.53	2	1.83	2.38	0.51	0.62	0.79	1.31	1.43	1.47	1.13
K_2O	5.91	3.52	5.75	5.98	4.45	2	2.16	3.12	2.96	3.1	3.05	3.86	4.09	4.08

to the stratigraphic column of the borehole, the lithology of the samples in this study mainly includes mudstone, sandstone, siltstone and few silty mudstone.

4.2 Trace elements

The trace element concentrations of the samples are listed in Table 2 and the Supplementary Data from Li et al. (2020).

4.2.1 Transition trace elements (TTEs) (Cu, Zn, Ni, Co, Sc, V, Cr)

Transition trace elements such as Ni, Co, Sc, V and Cr exhibit similar behaviors in magmatic process, but fractionate independently due to weathering (Feng and Kerrich, 1990). They were measured separately in this study. Strong positive correlation is found among Sc, V, Cr, Co, and Ni. The Sc and Co contents retain around the PAAS (Post-Archean Australian Shale) and UCC (Upper Continent Crust) values, but stay at the lower levels. The samples have lower Zn content than the PAAS and UCC values, except for two samples that have very high Zn content. Majority of the samples demonstrate a Cu content lower than the PAAS value but similar to the UCC value. The V and Cr contents are generally lower than the PAAS and UCC values.

4.2.2 Large-ion lithophile elements (LILEs) (Cs, U, th, Sr, Ba, Rb, Pb)

Large-ion lithophile elements such as Cs, Th and Rb are variable in abundance relative to PAAS and UCC. The average Cs and Th contents are lower than the PAAS and UCC values. The average Rb content is higher than PAAS and UCC values. The U content is generally similar to the PAAS and UCC values. The Ba content is about two orders of magnitude higher than the PAAS and UCC values for three samples from the Enping formation and three samples from the Wenchang formation. The samples (except for one) have Pb content higher than the PAAS and UCC values. Sr, Ba and Rb are probably common in alkali feldspar (e.g., Götze, 1998). Additionally, most samples reveal a significant Sr depletion relative to UCC, consistent with the relative Ca depletion, which implies that plagioclase minerals in the source rocks of these samples were decomposed due to weathering (Gao and Wedepohl, 1995).

4.2.3 High field-strength elements (HFSEs) (Nb, ta, Zr, Hf, Y)

High field-strength elements such as Zr, Nb, Hf and Y are preferentially partitioned into melts during crystallization and anatexis (Feng and Kerrich, 1990); therefore, they tend to be enriched in felsic rocks rather than mafic rocks. Most of the samples exhibit similar Nb, Ta, Hf and Y. The Zr content varies in a broad range, and a high Zr content may indicate recycled or fractionated sediments (McLennan et al., 1993). Hf is closely related to Zr, and both elements are controlled by zircon, which is fractionated by sorting due to resistance to weathering and high specific gravity (El-Bialy, 2013). The average Hf concentration for the samples is lower than PAAS and UCC, while the average Nb and Y concentrations are lower than PAAS but higher than UCC.

As shown in the Supplementary Data (S1) in this study, the vertical distributions of U_{EF}, V_{EF}, Cr_{EF}, Co_{EF}, Ni_{EF}, Cu_{EF}, Zn_{EF},

TABLE 2 Results of trace elements contents of the Eocene mudstones from the well of PY27, PY33, BY13, LH29, and LW21 in the Baiyun sag.

Well name	PY27	PY33	PY33	PY33	BY13	LH29	LH29	LW21	LW21	LW21	LW21	LW21	LW21	LW21
Formation	Enping	Enping	Enping	Enping	Enping	Enping	Enping	Enping	Enping	Enping	Wenchang	Wenchang	Wenchang	Wenchang
Depth	4628.6 m	4293.2 m	4295 m	5091 m	2653 m	3110–3119 m	3140–3149 m	3586–3589 m	3646–3649 m	3667–3669 m	3763–3766 m	3865–3868 m	3949–3952 m	4048–4050 m
Li	27.85	218.9	158.9	44.50	168.8	61.89	70.09	70.84	92.49	82.97	86.11	32.75	28.78	24.43
Be	3.53	3.80	6.91	5.48	3.39	1.96	1.95	3.06	2.90	3.15	2.73	2.38	2.20	2.62
Sc	13.13	14.57	16.25	14.98	10.88	11.49	12.97	12.43	11.91	13.04	13.67	13.13	12.67	11.93
Ti	4642	4921	5920	5164	3426	3092	3715	3273	2972	3548	3594	4661	4712	3519
V	98.51	104.9	111	106.5	87.13	80.94	87.6	107.2	101.5	93.8	90.09	89.31	84.45	70.07
Cr	43.57	69.53	74.09	62.49	15.98	52.95	55.51	66.03	52.62	50.45	40.52	40.27	36.52	30.54
Co	17.41	8.91	5.39	10.21	10.62	10.11	10.52	10.96	8.73	11.36	10.98	11.91	13.00	8.91
Ni	13.20	21.43	17.17	19.73	6.98	36.21	31.13	37.93	30.07	27.60	30.55	21.34	17.27	15.73
Cu	18.49	25.51	21.09	28.90	22.72	21.61	21.45	32.84	30.14	20.37	22.99	15.97	15.90	15.15
Zn	47.58	85.86	91.63	81.67	118.3	92.00	185.7	108.4	76.91	81.63	123.9	101.1	87.94	105.8
Ga	21.27	23.94	29.72	24.14	28.31	15.86	18.20	21.35	20.62	21.78	22.42	20.30	19.43	20.19
As	4.60	5.95	6.46	7.40	1.98	9.14	7.63	12.18	9.73	11.90	6.90	9.74	10.94	14.57
Rb	225.9	217.5	312.2	291.3	176.4	105.9	111.0	187.1	177.8	172.5	167.4	164.6	149.3	182.3
Sr	83.93	103.0	135.8	126.4	163.9	310.2	307.9	241.3	117.2	103.9	151	65.44	52.44	97.42
Y	28.97	41.88	30.27	42.02	10.05	16.54	18.96	22.77	22.43	23.48	21.08	24.89	22.96	25.91
Zr	443.1	238.2	220.9	290.2	156.6	103.5	147.4	112.1	90.72	116.2	103.6	428.2	279.8	202.4
Nb	16.71	22.20	26.52	22.37	8.61	9.50	11.50	14.39	12.26	14.59	13.25	16.09	16.08	16.27
Mo	1.58	0.76	0.82	0.46	1.17	2.82	2.34	1.12	0.73	1.20	1.40	1.07	1.24	1.60
Cd	0.08	0.04	0.09	0.21	0.12	0.16	0.26	0.14	0.10	0.06	0.10	0.07	0.10	0.13
Sn	4.15	7.07	8.31	6.36	1.29	2.80	2.89	4.99	4.46	4.75	3.87	3.59	3.11	3.72
Cs	15.37	32.30	39.39	32.32	20.76	11.85	9.94	23.71	22.96	21.61	13.50	7.70	6.56	9.16
Ba	596.4	484.8	1159	501.6	728.8	486.3	558.7	1348.	717.3	1121	1006	1148	763.6	2836
La	42.15	49.73	57.18	57.68	31.51	24.10	29.99	38.35	35.84	42.84	38.70	47.97	41.39	43.42
Ce	81.05	97.36	103.4	114.4	58.71	53.16	66.06	81.49	76.04	88.51	80.33	97.99	81.86	89.40
Pr	9.05	10.66	10.89	12.64	5.58	5.50	6.79	8.37	8.03	9.51	8.47	10.61	9.12	9.50
Nd	33.63	40.27	38.80	47.32	20.12	20.71	25.32	31.14	29.74	35.10	31.58	39.50	33.77	35.16
Sm	6.26	8.14	6.86	9.42	3.43	4.04	4.93	5.85	5.73	6.58	5.80	7.46	6.25	6.74
Eu	1.26	1.29	1.20	1.80	0.95	0.83	0.99	1.07	1.05	1.16	1.06	1.28	1.24	1.20

(Continued on following page)

10.3389/feart.2023.1177240

TABLE 2 (*Continued*) Results of trace elements contents of the Eocene mudstones from the well of PY27, PY33, BY13, LH29, and LW21 in the Baiyun sag.

Well name	PY27	PY33	PY33	PY33	BY13	LH29	LH29	LW21	LW21	LW21	LW21	LW21	LW21	LW21
Formation	Enping	Enping	Enping	Enping	Enping	Enping	Enping	Enping	Enping	Enping	Wenchang	Wenchang	Wenchang	Wenchang
Depth	4628.6 m	4293.2 m	4295 m	5091 m	2653 m	3110–3119 m	3140–3149 m	3586–3589 m	3646–3649 m	3667–3669 m	3763–3766 m	3865–3868 m	3949–3952 m	4048–4050 m
Gd	5.06	7.17	5.82	8.39	2.69	3.61	4.32	4.93	4.90	5.22	4.85	6.07	5.30	5.81
Tb	0.77	1.18	0.90	1.26	0.35	0.54	0.67	0.76	0.74	0.78	0.74	0.89	0.80	0.89
Dy	4.84	7.14	5.21	7.50	1.97	3.20	3.75	4.36	4.30	4.51	4.14	4.96	4.44	5.00
Ho	1.02	1.44	1.03	1.48	0.37	0.62	0.70	0.84	0.83	0.88	0.79	0.94	0.83	0.96
Er	3.20	4.29	3.06	4.38	1.03	1.81	2.04	2.44	2.41	2.57	2.26	2.72	2.45	2.74
Tm	0.50	0.63	0.45	0.63	0.15	0.26	0.29	0.35	0.36	0.38	0.33	0.41	0.36	0.40
Yb	3.60	4.26	2.99	4.30	1.04	1.77	2.08	2.38	2.37	2.56	2.22	2.91	2.49	2.76
Lu	0.55	0.62	0.44	0.63	0.16	0.26	0.30	0.34	0.35	0.37	0.32	0.44	0.38	0.40
Hf	11.15	6.46	5.93	7.64	4.25	2.85	4.00	3.11	2.67	3.27	2.92	10.70	7.31	5.32
Ta	1.38	2.04	2.29	1.93	0.58	0.75	0.87	1.22	1.02	1.20	1.01	1.23	1.22	1.22
Tl	1.03	1.15	1.54	1.32	0.90	0.53	0.55	1.03	0.91	0.83	0.84	0.85	0.76	0.95
Pb	23.78	35.93	38.55	32.80	30.09	21.14	22.30	39.15	37.41	34.56	32.26	25.75	22.13	42.01
Bi	0.46	1.09	1.29	0.95	0.32	0.42	0.43	0.82	0.77	0.78	0.63	0.50	0.50	0.54
Th	17.01	28.43	32.01	26.13	13.51	12.13	13.96	20.27	19.21	20.69	18.89	22.09	17.16	19.59
U	5.07	6.66	7.38	7.10	5.15	2.73	3.09	3.61	3.82	3.27	3.12	4.31	3.55	3.79
∑REE	221.91	276.05	268.48	313.85	138.10	136.96	167.19	205.44	195.10	224.45	202.68	249.04	213.64	230.28
∑LREE/∑HREE	3.57	3.02	4.35	3.45	6.76	3.79	4.05	4.25	4.04	4.51	4.52	4.63	4.34	4.13
$(La/Sm)_N$	4.23	3.84	5.25	3.85	5.78	3.75	3.82	4.13	3.93	4.10	4.20	4.05	4.16	4.05
La/Yb	11.72	11.68	19.12	13.43	30.33	13.59	14.42	16.09	15.10	16.72	17.42	16.50	16.60	15.71
$(La/Yb)_N$	7.90	7.87	12.89	9.05	20.45	9.16	9.72	10.85	10.18	11.27	11.74	11.13	11.19	10.59
$(Gd/Yb)_N$	1.14	1.36	1.57	1.58	2.09	1.64	1.67	1.67	1.66	1.65	1.76	1.68	1.71	1.70
δEu	0.67	0.50	0.57	0.61	0.92	0.65	0.64	0.59	0.59	0.59	0.59	0.57	0.64	0.57
δCe	0.95	0.97	0.94	0.98	0.99	1.07	1.07	1.05	1.04	1.01	1.02	1.00	0.97	1.02

10.3389/feart.2023.1177240

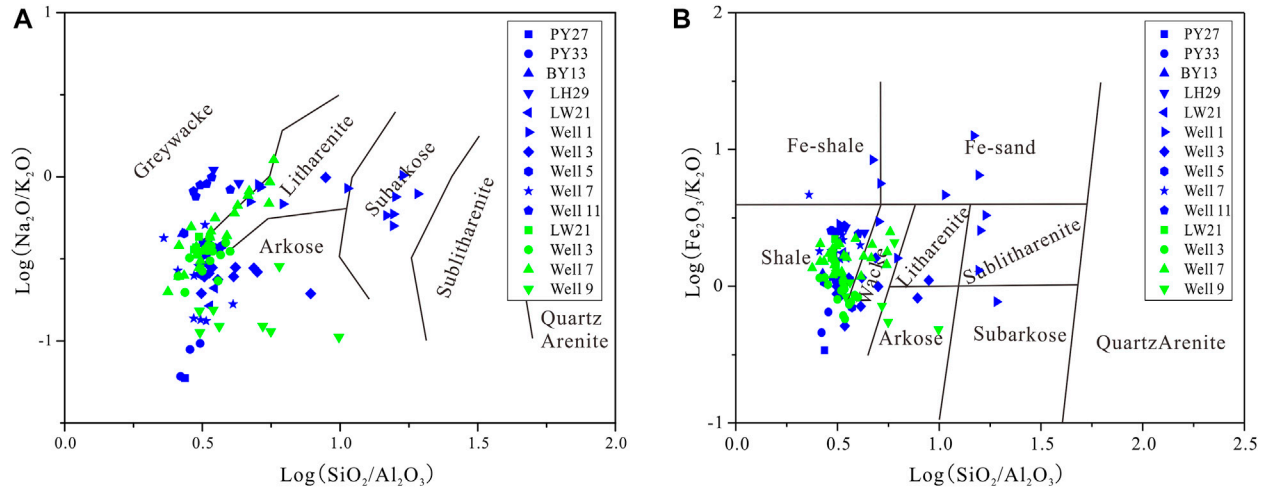

FIGURE 3
Geochemical classification of the mudstone samples on a log(SiO_2/Al_2O_3) vs. log(Na_2O/K_2O) diagram **(A)**; after Pettijohn et al., 1972) and a log(SiO_2/Al_2O_3) vs. log(Fe_2O_3/K_2O) diagram **(B)**; after Herron, 1988), the data of well 1, 3, 5, 7, 9 and 11 are from Li et al. (2020), the samples of Wenchang Formation are in green colour and Enping Formation are in blue colour and the following figures are the same.

Mo_{EF} and Mn_{EF} are as follows: U_{EF} (0.73–2.45, avg. 1.38), V_{EF} (0.27–0.74, avg. 0.51), Cr_{EF} (0.09–5.61, avg. 0.52), Co_{EF} (0.18–7.07, avg. 1.01), Ni_{EF} (0.09–7.88, avg. 0.63), Cu_{EF} (0.28–12.81, avg. 0.82), Zn_{EF} (0.46–35.3, avg. 2.23), Mo_{EF} (0.4–184, avg. 6.3), Mn_{EF} (0.08–7.98, avg. 0.73). It can be seen that Mo is strongly enriched, U and Zn are moderately enriched, and Co is weakly enriched.

4.3 Rare Earth elements (REEs)

The ΣREE ranges from 42.03 to 327.77 ppm (avg. 202.38 ppm) (Table 2). The ΣLREE/ΣHREE ratio is 1.15–4.87 (avg. 3.85) for the Wenchang samples and 3–6.76 (avg. 3.97) for the Enping samples (Table 2). The chondrite-normalized REE patterns of the samples from Wells PY27, PY33, BY13, LH29 and LW21 exhibit enrichment of LREE ($(La/Sm)_N$=3.75–5.78; La/Yb=11.68–30.33; $(La/Yb)_N$=7.87–20.45) and almost flat distribution of HREE ($(Gd/Yb)_N$=1.14–2.09 or avg. 1.63) (Figure 4). The Eu/Eu* anomaly generally varies from 0.5 to 0.92 (averaging 0.629) (Table 2). The Ce/Ce* anomaly varies from 0.94 to 1.07 (average 1.01) (Table 2). The REE patterns of other samples from Wells 1, 3, 5, 7, 9 and 11 are described by Li et al. (2020).

5 Discussion

5.1 Paleoredox

Trace elements are sensitive to redox in sediments and controlled by the redox conditions during deposition, so their contents or ratios can be used to reconstruct the paleoredox environment (Jones and Manning, 1994; Deng et al., 2019; Zhang et al., 2020, Zhang et al., 2021 X.; Qadrouh et al., 2021; Hou et al., 2022; Wu et al., 2022). By studying the REE, Shields and Stille (2001) noted that diagenesis could change the Ce anomaly and lead to a stronger positive correlation between Ce/Ce^*_N and Eu/Eu^*_N as well as between Ce/Ce^*_N and ΣREE, and a negative correlation between Ce/Ce^*_N and Dy_N/Sm_N. Correlation results show that the samples from the Baiyun sag have a relatively poor correlation between Ce/Ce^*_N and Eu/Eu^*_N (R^2 of 0.0235), between Ce/Ce^*_N and ΣREE (R^2 of 0.0123) and between Ce/Ce^*_N and Dy_N/Sm_N (R^2 of 0.0306), which indicate the sediments in the Baiyun sag are in the stage of early diagenesis. Therefore, the influence of diagenesis on REE distribution can be ignored. The dissolution and precipitation amounts of U, Mo, Ni, V, Cr, Co, Fe, Cu, and Zn are variable in different redox environments (Jomes and Manning, 1994; Tribovillard et al., 2006; Zeng et al., 2015). U^{6+}, V^{5+}, Mo^{6+}, and Fe^{3+} easily migrate in oxic seawater, whereas U^{4+}, V^{3+}, Mo^{4+}, and Fe^{2+} easily precipitate under reducing conditions (Pan et al., 2020). The enrichment of Mo requires the presence of H_2S and the Fe-Mn (oxyhydr) oxides shuttle can accelerate this process (Perkins and Mason, 2015; Zhu et al., 2022). Hallberg (1976) believed that the (Cu+Mo)/Zn ratio is >2 in reducing environment and <2 in oxic environment. The basis of this parameter is that for sediment deposited in anoxic environments (H_2S present), the precipitation of Cu is more favourable than Zn due to the solubility products of their sulphides (Jones and Manning, 1994). The (Cu+Mo)/Zn ratio is 0.01–1.28 (avg. 0.3) for the Enping samples and 0.06–0.59 (avg. 0.25) for the Wenchang samples, indicating that the mudstones in the study area were mainly deposited under oxic conditions.

Ni and Cr are stable under various redox conditions, while V can precipitate under reduction conditions and dissolve under oxidation condition (Hatch and Leventhal, 1992; Arthur and Sageman, 1994). Under euxinic conditions, Cr will be reduced and exported to the sediments as insoluble Cr_2O_3 or $Cr(OH)_3$ in euxinic conditions (Algeo and Rowe, 2012; Yan et al., 2021). In an oxic environment, V is present mainly as V (V) in vanadate oxyanions (HVO_4^{2-} and $H_2VO_4^-$), while under anoxic/euxinic conditions, V (V) is reduced

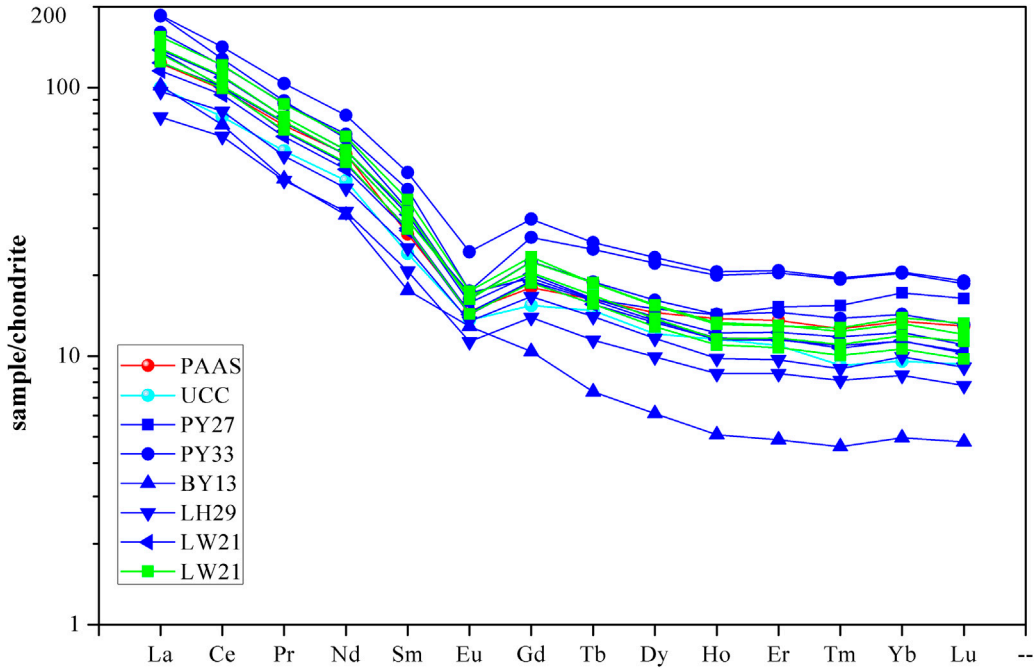

FIGURE 4
Chondrite-normalized rare Earth element patterns of the mudstone samples from the exploration well (PY27, PY33, BY13, LH29, and LW21) in the Baiyun sag.

to V(IV) by reaction with H_2S, humic acid, or fulvic acids, and precipitate in the sediments as an insoluble oxide (V_2O_3) or hydroxide ($VO(OH)_2$, $V(OH)_3$) phase (Perkins and Mason, 2015; Pan et al., 2020; Yan et al., 2021). Moreover, these H_2S and acids are derived mainly from the evolution of organic matter (Pan et al., 2020). Both Ni and V can be fixed in sediments by the formation of tetrapyrrole complexes and is a common constituent in crude oils (Jones and Manning, 1994; Perkins and Mason, 2015). Therefore, the ratios of V/(V+Ni), V/Cr, Ni/Co are effective indicators of redox conditions (Jones and Manning, 1994; Tribovillard et al., 2006). Previous studies proposed different criteria for V/(V+Ni), according to Hatch and Leventhal (1992) and Wu et al. (2022), a high V/(V+Ni) value (≥0.84) reflects water column stratification and indicate anoxic bottom water, and this value range from 0.54 to 0.72 reflects a dysoxic environment with weak stratification of the water column, while a low value (0.46–0.60) reflects an oxic environment. In this study, V/(V+Ni) <0.6 indicates an oxygen-rich environment, V/(V+Ni) of 0.6–0.84 reflects an oxygen-poor environment with weak water stratification, and V/(V+Ni) >0.84 indicates an anaerobic reduction environment with water stratification (Zhang et al., 2020). V/Cr <2 indicates an oxygen-rich environment, V/Cr of 2–4.25 indicates an oxygen-poor weak reducing environment, and V/Cr >4.25 indicates a strong reduction environment (Zhang X. et al., 2021). Moreover, Ni/Co <5.0 reflects an oxidizing environment, Ni/Co of 5.0–7.0 reflects a suboxic to dysoxic environment, and Ni/Co >7.0 reflects a reducing environment (Jones and Manning, 1994). As shown in S1 in this study, and Figures 5, 6, the V/(V+Ni) ratio is 0.71–0.91 (avg. 0.82) and 0.15–0.93 (avg. 0.68) for the Wenchang and Enping samples, respectively, which suggests that the oxidability of the water body was stronger during the deposition of the Enping formation than that of the Wenchang formation.

The V/Cr ratio is 0.94–5.05 (avg. 2.39) for the Wenchang samples and 0.12–6.6 (avg. 1.56) for the Enping samples (S1), suggesting that both formations were deposited in an oxygen to oxygen-poor environment. The Ni/Co ratios of the Wenchang and Enping samples are 0.04–3.33 (avg. 1.31) and 0.22–10.43 (avg. 2.31) (S1), respectively, indicating an oxidizing environment.

Both Th and U are oxychalcophile lithophile elements. U exists as dissolved U^{6+} in oxidized water, and the dissolved U^{6+} in reduced water is often reduced to insoluble U^{4+}, forming autogenous U minerals (Langmuir, 1978; Calvert and Pedersen, 1993; Jones and Manning, 1994; Kimura and Watanabe, 2001; Cao et al., 2021). In contrast, Th exists as soluble Th^{4+} regardless of highly reducing conditions or oxidizing environments and has usually a detrital origin associated with clay minerals (Zhang L. et al., 2021). U/Th can reflect redox conditions–the lower the value, the stronger the reducibility. U/Th <0.27 reflects an oxic environment, U/Th of 0.27–0.50 reflects a dysoxic condition, and U/Th >0.50 reflects an anoxic environment (Wignall and Twitchett, 1996). Figure 5, Figure 6 and S1 show that the U/Th ratios of the Wenchang and Enping samples are 0.15–0.32 (avg. 0.21) and 0.13–0.38 (avg. 0.22), respectively, suggesting an oxic environment. Moreover, (Cu+Mo)/Zn, V/(V+Ni), V/Cr and Ni/Co were also combined with U/Th to understand the depositional environment of the Wenchang and Enping formations. In Figures 7A–D, all (but a few) samples are plotted in a dysoxic–oxic environment, which is consistent with the results derived from the ratios of redox-sensitive trace metals. The same findings can be obtained from the diagrams of Ni/Co-V/Cr (Figure 7E) and Ni/Co-Mo (Figure 7F), which suggests a dysoxic to

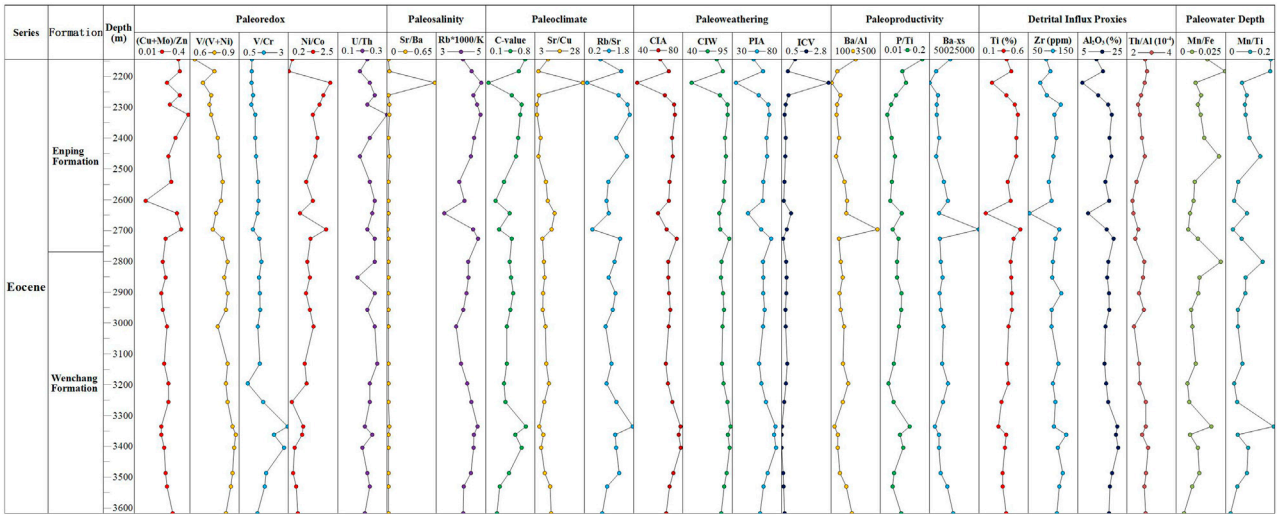

FIGURE 5
Vertical variations in paleoredox indices, paleosalinity indices, paleoclimate indices, paleoweathering indices, paleoproductivity indices, detrital influx proxies and paleowater depth for the mudstone samples in the Well 3.

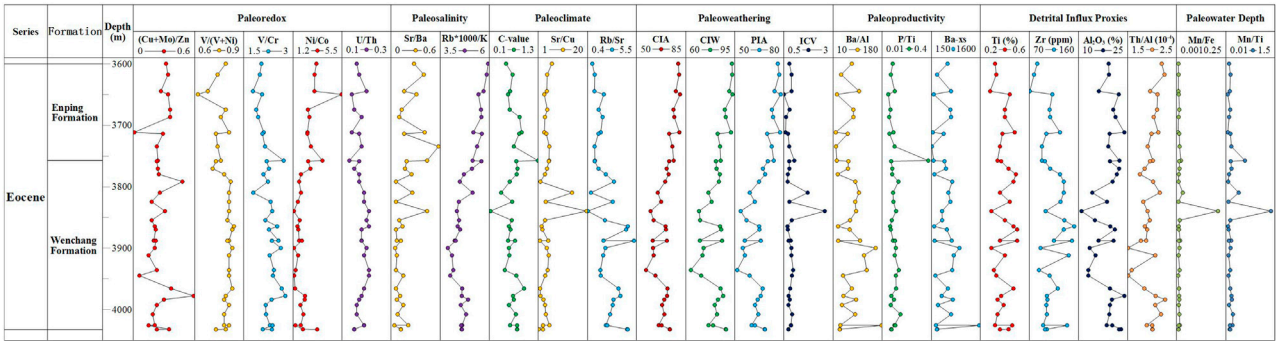

FIGURE 6
Vertical variations in paleoredox indices, paleosalinity indices, paleoclimate indices, paleoweathering indices, paleoproductivity indices, detrital influx proxies and paleowater depth for the mudstone samples in the Well 7.

oxic environment. Moreover, the paleoredox indices vary obviously in the vertical direction (Figure 5, Figure 6), and the ratios of V/(V+Ni), V/Cr and U/Th tend to decrease upward in the target intervals (Figure 5, Figure 6), implying a gradual evolution from weak oxidizing condition to strong oxidizing condition.

Some proxies, such as U_{EF}, V_{EF}, Cr_{EF}, Co_{EF}, Ni_{EF}, Cu_{EF}, Zn_{EF}, Mo_{EF}, Mn_{EF}, can be used to establish the specific redox thresholds and variations for sediments and/or sedimentary rocks, but they should be normalized and calibrated depending upon formations (Algeo and Maynard, 2004; Tribovillard et al., 2006; Algeo and Li, 2020; Liu et al., 2022). The enrichment factors (EFs) of elements shown in Figure 5, Figure 6 and S1 are calculated by: $X_{EF}=(X/Al)_{sample}/(X/Al)_{standard}$, where X_{EF} represents the enrichment factor of trace metal, and "standard" refers to PAAS. In practices, EF <1 represents depleted concentrations, EF >3 represents detectable enrichment over average crustal concentrations, and EF >10 represents moderate–strong enrichment (Tribovillard et al., 2006; Li L. et al., 2019). Additionally, the U_{EF}–Mo_{EF} plot (Algeo and Tribovillard, 2009; Li L. et al., 2019) is used for determining the redox degree, and it can also be used for identifying the water retention degree. For the Wenchang and Enping samples, U_{EF} is 0.92–2.16 (avg. 1.34) and 0.73–2.45 (avg. 1.42), respectively, and Mo_{EF} is 0.43–5.62 (avg. 1.12) and 0.4–184 (avg. 10.85), respectively (S1). All samples, except those from Well 1, show Mo_{EF} of 0.4–5.62 (avg. 1.26), close to UCC. On the U_{EF}–Mo_{EF} plot (Figure 8A), most samples show lower Mo/U values and fall into the range below 1 times the seawater (1×SW) and near the 0.3×SW line, reflecting predominantly suboxic conditions and less basin restriction.

Pr and Ph are important indicators of paleoenvironment. Pr/Ph <0.80 and Pr/Ph >3.00 indicate anoxic environment and oxic environment, respectively (Peters et al., 2005; Hakimi et al., 2011; Xu

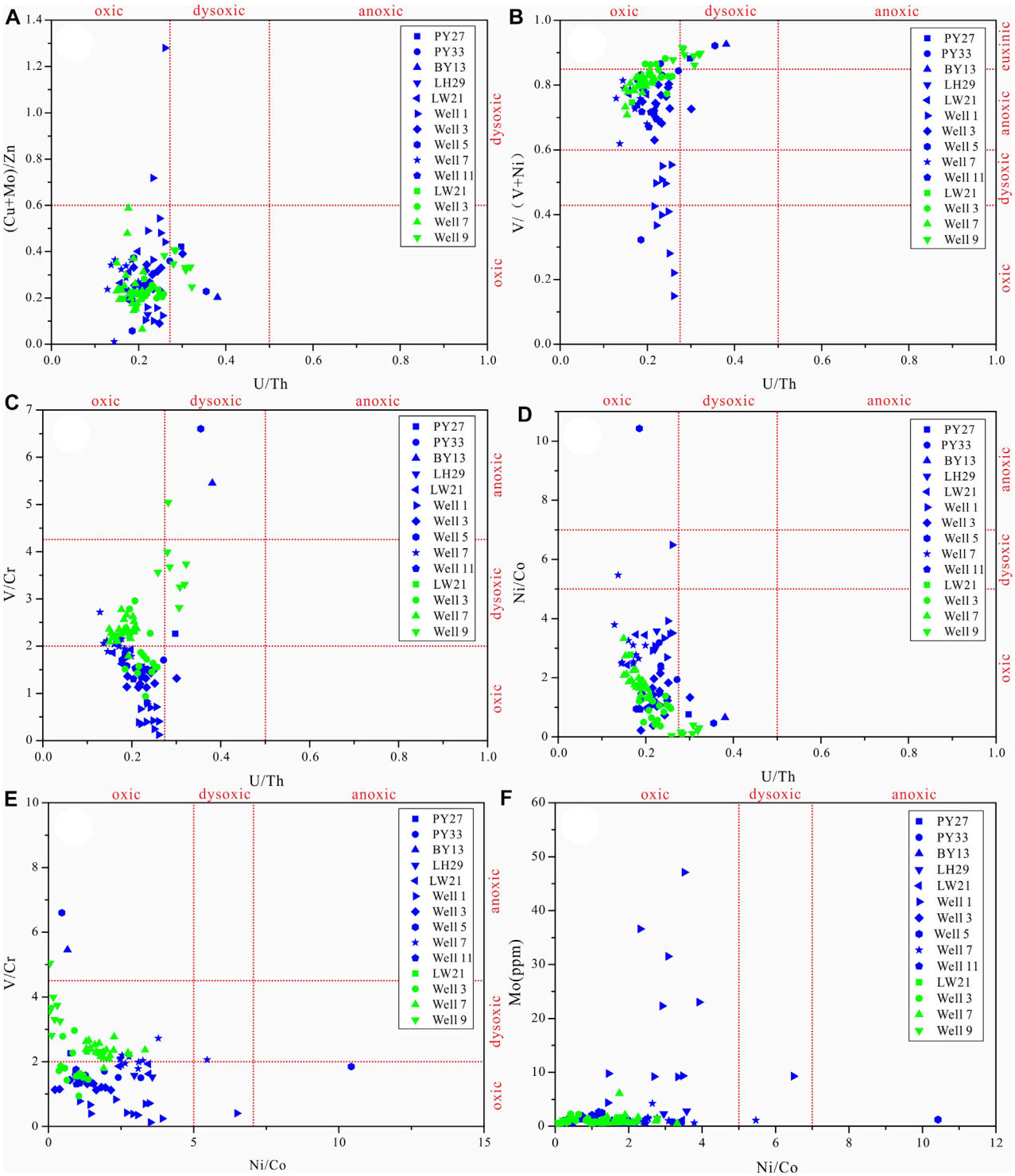

FIGURE 7
Bivariate plots of trace element ratios used as proxies to infer paleoredox conditions: **(A)** U/Th vs. (Cu +Mo)/Zn (adopted from Wang C. et al., 2018); **(B)** U/Th vs. V/(V + Ni); **(C)** U/Th vs. V/Cr; **(D)** U/Th vs. Ni/Co [**(B–D)** adopted from Ross and Bustin, 2009]; **(E)** Ni/Co vs. V/Cr; **(F)** Ni/Co vs. Mo. [**(E,F)** adopted from Qadrouh et al., 2021].

et al., 2016; Makeen et al., 2019; Xie et al., 2021; Wu et al., 2022). A few oil samples from the southwestern of the Baiyun sag reveal low Pr/Ph ratios (0.89–1.99) (Fu et al., 2019), and other oil samples from the Panyu uplift and the Baiyun sag mostly have the Pr/Ph ratios ranging from 3.14 to 8.06 (Wang C. et al., 2018; Fu et al., 2019, 2020), indicating that the parent material of crude oil in the Baiyun sag is mainly terrigenous humus organic material in an oxidizing environment. The Pr/n-C_{17}–Ph/n-C_{18} plot is also widely used to

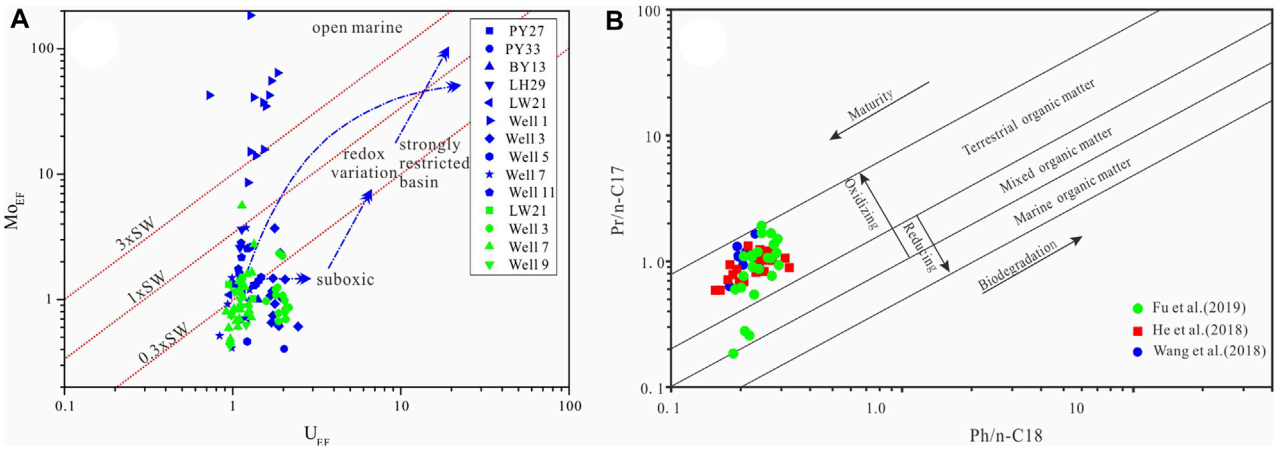

FIGURE 8
(A) U_{EF} *versus* Mo_{EF}. The lines with arrows indicate the evolution in Mo–U patterns in open marine environments, restricted basins, and setting with the operation of Fe–Mn shuttle (Algeo and Tribovillard, 2009). The dashed lines indicated multiples (0.3, one and 3) of the Mo/U ratios of the present-day seawater; **(B)** Cross plot of Pr/n-C_{17} vs. Ph/n-C_{18} for the oil in the Baiyun Sag. The boundary lines are after Shanmugam (1985).

indicate the redox conditions (Peters et al., 2005; Xu et al., 2016; Makeen et al., 2019; Xie et al., 2021). It can be inferred from Figure 8B that the source rock in the Baiyun sag was deposited in an oxic environment with the major contribution of terrigenous organic matter.

5.2 Paleosalinity

Salinity affects the water stratification in a lacustrine or marine basin and has a marked influence on the development of source rocks. The paleowater salinity is usually determined according to the differential accumulation of elements. Ba can precipitate after combining with other elements. Ba is less soluble, while Ba^{2+} is prone to combine with SO_4^{2-} to generate $BaSO_4$ which will precipitate (Sun et al., 2013; Song et al., 2017; Li L. et al., 2019; Zhang et al., 2020). Ba will precipitate at the bottom of water body when the salinity rises to a certain level, Sr can migrate more easily than Ba, and Sr will precipitate only when the salinity is very high (Xi et al., 2011; Fu et al., 2016; Wang Z. et al., 2018; Zhang et al., 2020). Usually, ratios of Sr/Ba>1 show saline water conditions, from 1.0 to 0.5 represent brackish-environments, and <0.5 indicate freshwater conditions (Meng et al., 2012; Deng et al., 2019; Sajid et al., 2020; Zhang et al., 2020; Zhang X. et al., 2021). Sedimentary Sr and Ba are easily remobilized during burial diagenesis. Sr may be released through diagenetic reaction of Sr bearing minerals, dehydration of clay minerals, or by degradation of organic host phases (Wei and Algeo, 2020a). The key issue of Sr/Ba ratios as paleosalinity proxy is potential alteration of the clay fraction signal by carbonate-hosted Sr, so it is significant to exclude the influence of carbonate-hosted Sr and then establish a maximum carbonate threshold (Wei and Algeo, 2020a; Zhang L. et al., 2021). To determine the Sr/Ba value, the carbonate-hosted Sr in sediments should be measured based on the CaO content (5%) (Wei and Algeo, 2020a; Zhang L. et al., 2021; Liu et al., 2022). Most of the samples contain CaO <5% and with no obvious relationships on the Sr/Ba–CaO plot (Figure 9). Thus, the presence of Sr in the samples is thought to have originated from clay-fraction instead of carbonate-hosted Sr, except for few samples with high CaO content. The Sr/Ba value is 0.02–0.44 (avg. of 0.08) for the Wenchang samples, and 0.01–0.72 (avg. 0.22) for the Enping samples, indicating that the Engping formation was deposited in fresh water environment (salt water environment occasionally) (especially for Well 11).

Rb/K is also an effective index for determining the salinity of paleowater (Zhang et al., 2020; Zhang X. et al., 2021). From fresh water to salt water, the content of kaolinite decreases, while the content of illite increases. Illite has the highest adsorption capacity for K and also a good adsorption capacity for other alkali metal ions (AMIs) such as Rb and Cs, while kaolinite has a poor adsorption capacity for AMIs and the lowest adsorption capacity for K (Zhang X. et al., 2021). Since the contents of Rb and K are not at the same order of magnitude, Rb multiplied by 1000 is used for calculation. Rb*1000/K <4 indicates fresh water environment, Rb*1000/K of four to six indicates brackish water environment, and Rb*1000/K >6 indicates marine water environment (Sajid et al., 2020; Zhang X. et al., 2021; Liu et al., 2022). Rb/K is determined to be 3.52–5.49 (avg. 4.4) for the Wenchang samples and 2.77–6.18 (avg. 4.82) for the Enping samples, suggesting that the Eocene strata in the Baiyun sag were deposited in a fresh–brackish water environment with an upward increase in salinity. The Sr/Ba–Rb*1000/K plot shows that most of the samples fall in the areas of fresh water and a few samples in the areas of brackish water, indicating the dominance of fresh water environment (Figure 10A). The Sr/Ba and Rb*1000/K values increase from the bottom to the top in wells 3 and 7, indicating that the Eocene strata in the Baiyun sag were deposited in a fresh–brackish water environment with an upward increase in salinity (Figures 5, 6), which may suggest the increased inflow of seawater into the lake.

Marine sedimentary rocks have higher B and lower Ga contents than those derived from fresh water environments. Hence, higher B/Ga value corresponds to higher salinity. Generally, B/Ga >5 indicates salt water environment, B/Ga of 2.five to five

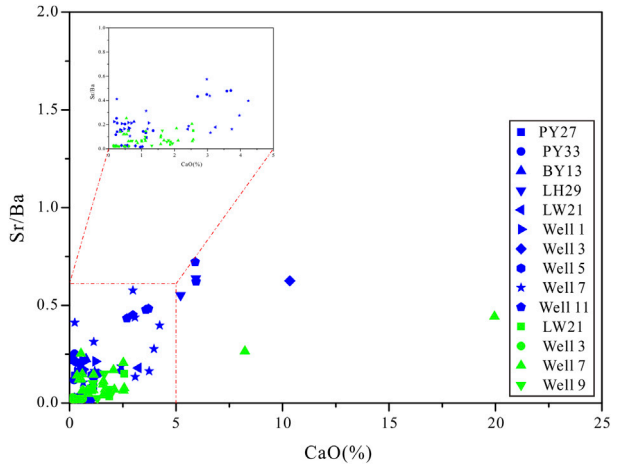

FIGURE 9
Correlation between Sr/Ba ratios and CaO content of the mudstone samples in the Baiyun sag.

indicates brackish water environment, and B/Ga <2.5 indicates fresh water environment (Wei et al., 2018; Deng et al., 2019). B/Ga is determined to be 0.36–1.24 (avg. 0.68) for the Wenchang samples and 0.78–2.02 (avg. 1.33) for the Enping samples, both lower than 2.5, indicative of fresh water environment. This finding is supported by the V/Ni–Sr/Ba plot (Figure 10B). Clay minerals can absorb boron from water and fix it. Quantity of boron absorbed is related to the concentration of boron in water (Walker, 1968; Zhang et al., 2017). The absorption is unidirectional, once fixed in clay minerals, boron can't be desorbed as its concentration decreases (Liu et al., 2015; Li et al., 2017). Therefore, the B content can indicate paleosalinity. "Equivalent boron" was proposed to quantitatively estimate the paleosalinity by the formula: Equivalent Boron = (11.8*T*8.5)/(K*1.7*(11.8-K)), where T is the B concentration in ppm and K is the K_2O concentration in wt% (Walker, 1968). The equivalent-boron ranges of 300–400, 200–300 and <200 ppm are indicative of marine water, brackish water, and fresh water environments, respectively (Degens and Ross, 1974). The equivalent-boron range is determined to be 27.19–97.39 (avg. 50.88) and 78.89–146.88 (avg. 111.14) for the Wenchang and Enping samples, respectively, indicating fresh water environment.

As the salinity of sedimentary water increases, the $\delta^{13}C$ and $\delta^{18}O$ values of carbonate cement increase, so C and O isotopes can also be used to estimate the paleosalinity and can also provide more reliable data than major and trace element analyses when rocks of different origins are involved (Keith and Weber, 1964; Dai et al., 2009; Deininger et al., 2012; Yan and Zheng, 2015; Li L. et al., 2019). The $\delta^{13}C$ values of the sandstone samples vary from -10.9‰ to -7.2‰ (average -8.58‰) while $\delta^{18}O$ range between -18.4‰ and -14.5‰ (average -17.1‰). Previous research (Guo and Wang, 1999) has shown that $\delta^{13}C$<0‰ and $\delta^{18}O$>-10% indicate that the carbonate cements in the sandstones related to sulfate reduction in early diagenesis, while the $\delta^{13}C$ values higher than 0‰ reflect the carbonate cements related to biogas generated by methane bacteria, and the values of $\delta^{13}C$ <0‰ and $\delta^{18}O$<-10% indicate that oxidation of organic matter has as an important role in the occurrence of carbonate cements in the sandstone reservoirs. Therefore, carbonate cements of the sandstones in the Baiyun sag should be related to the oxidation of organic matter. Based on the isotope compositions of marine limestones and fresh water limestones formed since the Jurassic, the isotope coefficient Z is obtained by the formula: Z = 2.048 ($\delta^{13}C$+50) + 0.498 ($\delta^{18}O$+50), where Z is the paleosalinity in ‰ (Keith and Weber, 1964). Usually, Z >120‰ indicates marine (or continental saline lake) environment, and Z <120‰ indicates continental fresh water environment (Keith and Weber, 1964; Zhang et al., 2020). In this study, Z is determined to be 96.51‰–104.51‰ (avg. 101.24‰) for the Engping samples (Table 3), indicating continental fresh water environment. It is thus inferred that the Eocene strata in the Baiyun sag were deposited in a fresh–brackish water environment, with the paleosalinity increasing from the Wenchang formation to the Enping formation (Figure 5, Figure 6).

5.3 Paleoclimate

Paleoclimate can be recorded by the distribution, composition and relative concentration of some trace elements (e.g., Fe, Mn, Cr, Ni, V, Co, Ca, Mg, Sr, Ba, K, Na, Cu and Rb) in mudstones (Worash, 2002). The C-value is used as an indicator of paleoclimate (warm and humid or hot and arid), which is defined as follows: C-value=Σ(Fe+Mn+Cr+Ni+V+Co)/Σ(Ca+Mg+Sr+Ba+K+Na) (Zhao et al., 2007; Cao et al., 2012). This value is based on the hypothesis that Fe, Mn, Cr, Ni, V, and Co are enriched under humid circumstances. However, in an arid environment, as water alkalinity increases due to evaporation, saline minerals precipitate; as a result, Ca, Mg, K, Na, Sr and Ba are enriched (Zhao et al., 2007; Cao et al., 2012; Tao et al., 2017; Deng et al., 2019). Generally, C value >0.8 indicates humid climate, 0.2<C value<0.8 indicates semi-humid to semi-arid climate, and C value <0.2 indicates arid climate (Awan et al., 2020). In this study, the C-value is determined to be 0.13–0.95 (avg. 0.56) and 0.14–5.73 (avg. 0.84) for the Wenchang and Engping samples, respectively, and most of the samples have the C-values ranging from 0.2 to 0.8, suggesting a semi-humid to semi-arid climate (Figure 11). Sr/Cu is proposed as a geochemical indicator of paleoclimate (Lerman, 1978). Generally, Sr/Cu ≤10 indicates warm and humid climate, and Sr/Cu ˃10 indicates hot and dry climate (Lerman, 1978; Jia et al., 2013b; Fu et al., 2016; Tao et al., 2017; Zhang et al., 2020). The Sr/Cu ratios of the Wenchang and Enping samples suggest that the Eocene strata in the Baiyun sag were deposited in a warm and humid climate. Sr/Rb is also used to reflect the paleoclimate. Rb remains stable in weathering process, similar to Cu, while Sr often precipitates in warm and humid climate. The Rb/Sr ratio is variable depending upon the climate: high Rb/Sr ratios reflect cold climate, and low Rb/Sr ratios reflect warm climate (Chen et al., 2001; Bai et al., 2015; Zhang X. et al., 2021). The Rb/Sr ratios of the Wenchang and Enping samples show an opposite trend to Sr/Cu and C-value (Figure 5, Figure 6), suggesting humid climate. Heavy precipitation and flourishing vegetation in a warm and humid climate could provide abundant organic matters for the source rocks (Meng et al., 2012). This assumption is verified by the Al_2O_3+K_2O+Na_2O–SiO_2 plot (Figure 12A) and the K_2O/Al_2O_3–Ga/Rb plot (Figure 12B), which suggest that the samples

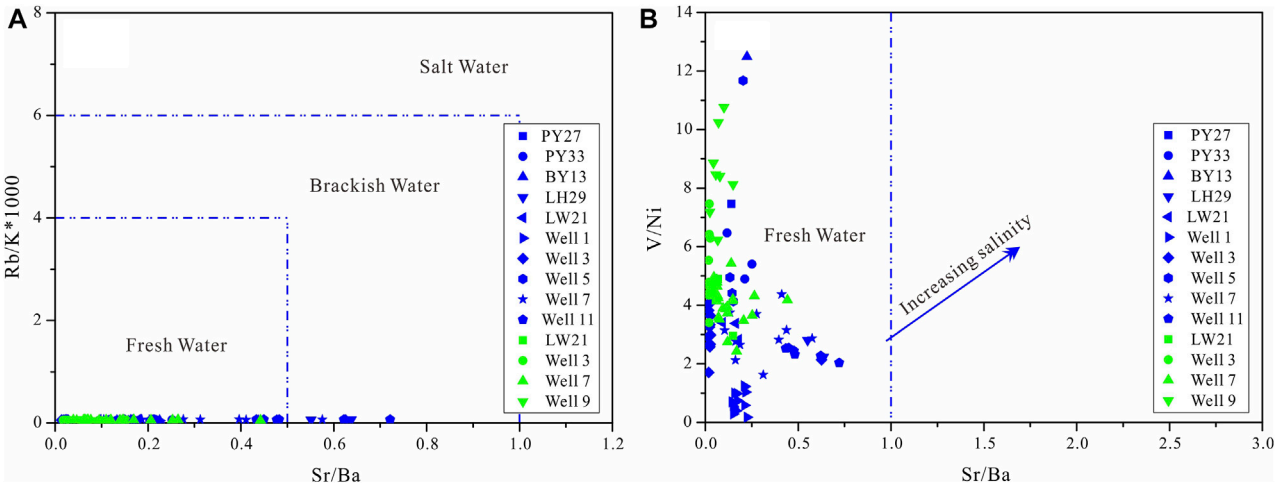

FIGURE 10
(A) Paleosalinity scatter plots of Sr/Ba and Rb/K; **(B)** Sr/Ba *versus* V/Ni showing the depositional environment (adopted after Jia et al., 2013a).

TABLE 3 $\delta^{13}C$ and $\delta^{18}O$ values of carbonate cement for the sandstone samples for Enping formations in the Baiyun sag.

Well name	Formation	Depth m)	$\delta^{13}C_{PDB}$(%)	$\delta^{18}O_{PDB}$(%)	Z value
PY27	Enping	4142.75	-8.1	-18.1	101.7
PY27	Enping	4148.76	-10.9	-17	96.51
PY27	Enping	4629.6	-7.6	-18.2	102.67
PY27	Enping	4630.25	-7.2	-18.4	103.39
PY27	Enping	4630.43	-8.1	-18	101.75
PY33	Enping	4298.1	-7.6	-14.5	104.51
PY33	Enping	4300.6	-10.7	-17.7	96.57
PY33	Enping	4302.01	-8.4	-14.6	102.83

have largely experienced semi-arid/warm climatic conditions. It is thus inferred that the Eocene strata in the Baiyun sag were deposited in a transitional (semi-arid to semi-humid) climate, with a gradually increasing temperature during the early deposition of the Wenchang formation (Figure 5, Figure 6).

5.4 Paleoweathering

Paleoweathering can be reconstructed from various geochemical parameters. The chemical index of alteration (CIA) is proposed to estimate the intensity of weathering depending upon the transformation of feldspar into clay minerals (Nesbitt and Young, 1982, 1984). CIA is defined as: $CIA=[(Al_2O_3)/(CaO^*+Na_2O+K_2O+Al_2O_3)]\times100$ (in molecular proportions), where Cao* represents CaO associated with the silicate fraction of the sample. When $Cao^*<Na_2O$, Cao* is directly used; otherwise, $Cao^*=Na_2O$ (McLennan et al., 1983; Oyebanjo et al., 2018; Chi et al., 2021). CIA of 50–60 indicates incipient weathering, CIA of 60–80 indicates intermediate weathering, and CIA >80 indicates extreme weathering (Fedo et al., 1995). In this study, CIA is determined to be 56.73–82.71 (avg. 70.31) for the Wenchang samples and 37.55–81.68 (avg. 66.76) for the Enping samples (S1; Figure 13), mostly higher than UCC (UCC=48; Rudnick and Gao, 2003) but lower than PAAS (70–75; McLennan et al., 1993). It is thus inferred from CIA values that the Eocene strata in the Baiyun sag undergone mild to moderate chemical weathering. As shown in the Al_2O_3–(CaO^*+Na_2O) –K_2O (A-CN-K) triangle (Figure 14A), majority of the Wenchang and Enping samples exhibits the values parallel to the A-CN line and between the weathering trend lines of granodiorite and granite (Figure 14A), implying that they undergone mild to moderate weathering. The degree of chemical weathering can also be estimated by using the chemical index of weathering (CIW) (Harnois, 1988), which is similar to CIA except for the exclusion of K_2O and hence not sensitive to post-depositional K-enrichment. CIW is defined as: $CIW=[Al_2O_3/(Al_2O_3+CaO^*+Na_2O)]\times100$. CIW is 80 for unweathered potassic granite and 100 for fresh K-feldspar (Fedo et al., 1995). In this study, CIW is determined to be 63.67–93.29 (avg. 83.53) for the Wenchang samples and

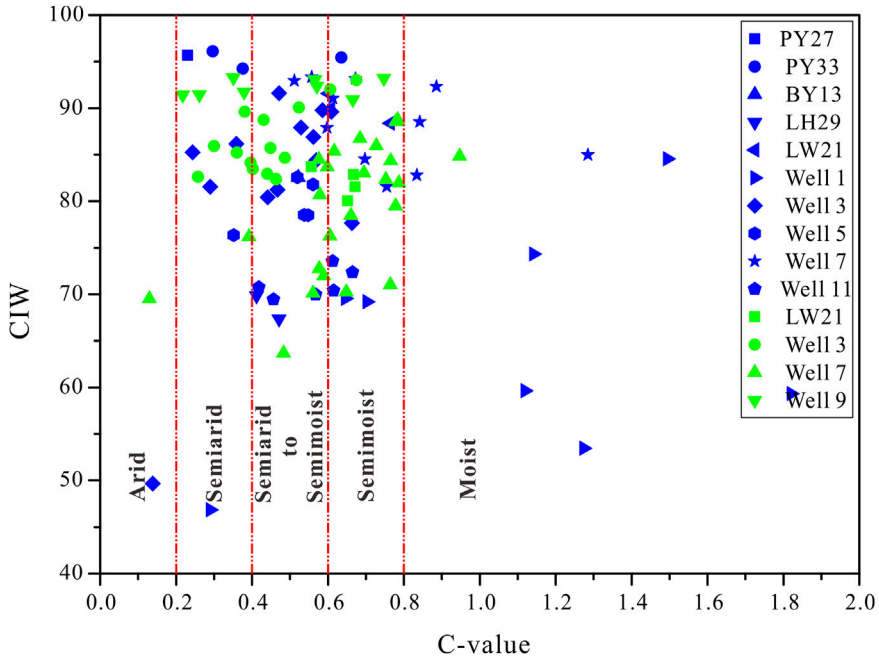

FIGURE 11
The C-value (Σ (Fe+Mn+Cr+Ni+V+Co)/Σ (Ca+Mg+Sr+Ba+K+Na)) of the mudstone samples from the Baiyun sag, reflecting paleoclimate. The distinguishing criteria are after Zhao et al. (2007).

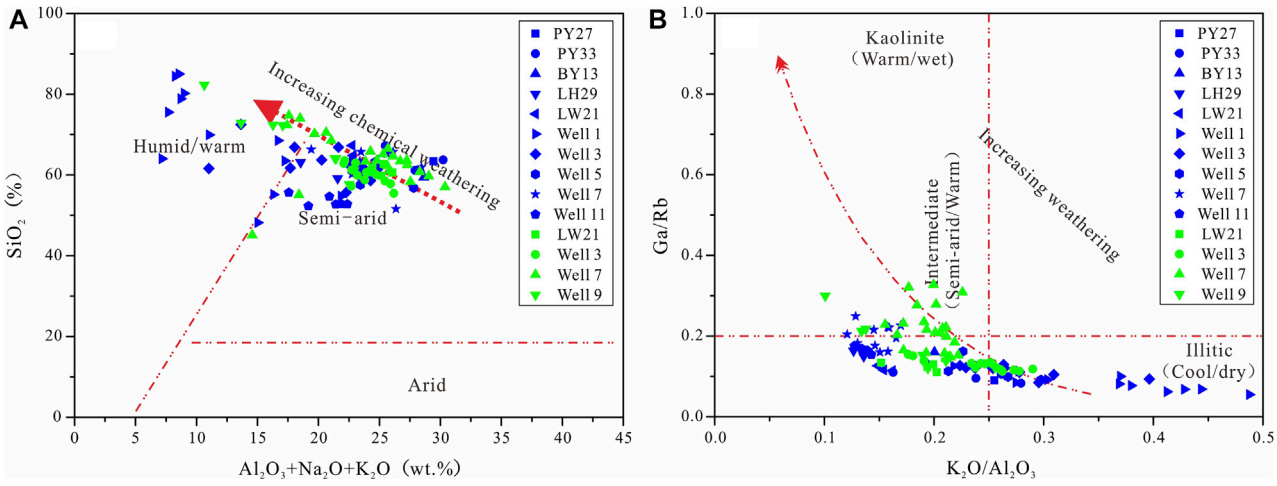

FIGURE 12
Discrimination diagrams of **(A)** (Al_2O_3+K_2O+Na_2O) vs. SiO_2 (base map after Suttner and Dutta., 1986) and **(B)** K_2O/Al_2O_3 vs. Ga/Rb (base map after Roy and Roser, 2013) for the mudstone samples of Baiyun sag.

46.85–96.11 (avg. 79.49) for the Enping samples, indicating moderate chemical weathering. The plagioclase index of alteration (PIA) is another indicator of chemical weathering, which precludes the influence of K-metasomatism (Fedo et al., 1995). PIA is defined as: PIA=100×(Al_2O_3−K_2O)/(Al_2O_3+CaO*+Na_2O−K_2O). PIA for the Wenchang and Engping samples is 51.44–80.99 (avg. 64.74) and 22.07–78.59 (avg. 60.09), respectively, revealing moderate chemical weathering (S1). These results support the early conclusion that the study area experienced mild to moderate chemical weathering as indicated by the A-CN-K diagram.

Moreover, the index of compositional variability (ICV) is proposed to measure the compositional maturity of mudstone, and it is defined as: ICV=(Fe_2O_3+K_2O+Na_2O+CaO+MgO+MnO+TiO_2)/Al_2O_3), where $Fe_2O^t_3$ = total iron and CaO includes all sources of Ca (Cox et al., 1995). Generally, immature sediments containing a high

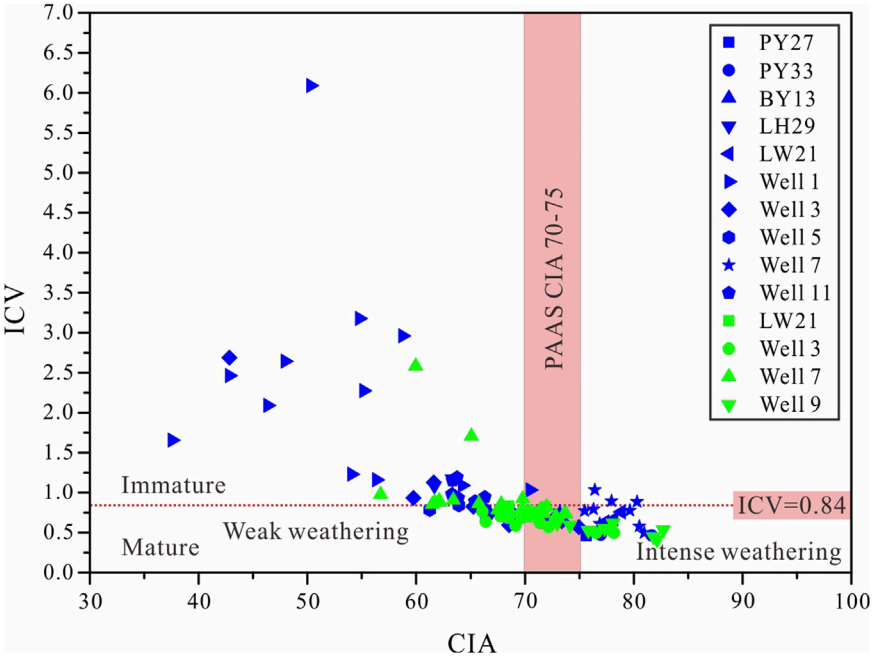

FIGURE 13
CIA vs. ICV diagram for the mudstone samples in the Baiyun sag (after Nesbitt and Young, 1984; Cox et al., 1995).

proportion of silicates other than clays show high ICV values, whereas mature sediments, depleted in silicates other than clay commonly show low ICV values (Ma et al., 2022). Therefore, ICV >0.84 reflects rock-forming minerals such as plagioclase, K-feldspar, amphibole, and pyroxene, indicative of first-cycle deposits (Van de Kamp and Leake, 1985), and ICV <0.84 is indicative of weathered detrital minerals (Cox et al., 1995) and recycling processes (Madhavaraju et al., 2016). The Enping samples exhibit higher ICV values (0.46–6.09, avg. 1.14) than the Wenchang samples (0.41–2.58, avg. 0.77). There are more sandstone samples in Enping Formation than in Wenchang Formation, and mudstones have experienced stronger weathering than sandstones, this is why the weathering indexes of Enping Formation are lower.

The relationship between Th/Sc and Zr/Sc can be used to deduce mineral selection, sediment recycling, and whether the source rocks are mantle or crustal-derived (McLennan et al., 2003; Zaid, 2015; González et al., 2017). Zr/Sc and Th/Sc of the samples in this study are 3.51–33.75 (avg. 9.62) and 0.63–3.05 (avg. 1.68), respectively. On the Zr/Sc–Th/Sc plot (Figure 14B), the samples are plotted in the region subparallel to Trend one and above UCC, implying a greater contribution of felsic sources, which suggests slight to moderate recycling.

5.5 Paleoproductivity

Paleoproductivity plays an important role in the formation and distribution of effective source rocks, and it is mainly controlled by the supply of nutrient elements including the remains of aquatic organisms and the clasts of terrestrial plants (Zhang X. et al., 2021). The trace elements (e.g. Ba, P, Cu, Zn and Ni) are usually used to reconstruct the paleoproductivity (Holland, 1978; Algeo et al., 2011; Chi and Liu, 2020; Zhang X. et al., 2021; Liu et al., 2022). Ba content is a good geochemical indicator for paleoproductivity: higher Ba content is correlated with higher productivity (Paytan and Griffith, 2007; Yeasmin et al., 2017; Li Y. et al., 2019). Ba/Al can also be used to quantify the paleoproductivity (Chen et al., 2016). Ba/Al is determined to be 26.37–1544.53 (avg. 352.27) and 19.52–3302.74 (avg. 273.69) for the Wenchang and Enping samples, respectively. The average value of Ba/Al for samples from wells except 3 and 9 is lower than that (100–200) of cores from the modern continental margin of Central California (Dean et al., 1997), indicating medium to high productivity. Moreover, the excess barium (Ba_{xs}) is a useful indicator for primary productivity reconstruction. Ba_{xs} is calculated as follows: $Ba_{xs}=Ba_{sam}-Ba_{sam}\times Al_{sam}/Al_{PAAS}$, where Ba_{sam} and Al_{sam} represent the Ba and Al concentrations of the samples, respectively, and Al_{PAAS} represents the average concentration of Al in PAAS. Ba_{xs} values >1000 ppm, of 200–1000 ppm, and <200 ppm indicate high, medium, and low paleoproductivity, respectively (Yi et al., 2007). Ba_{xs} is 237.09–12202.32 (avg. 2705.21) for the Wenchang samples and 169.87–24946.78 (avg. 1915.84) for the Enping samples. Except for samples from Well three and Well 9, the Ba_{xs} values of the samples from other wells are almost lower than 1000, suggesting medium to high productivity (Figure 15A). P is a nutrient necessary for the growth of plankton, and it can be used to estimate ancient bioproductivity (Holland, 1978; Tyrrell, 1999; Hou et al., 2022). Therefore, P concentration is widely used to analyse the paleoproductivity, and P/Ti is effective for offsetting the effect of terrigenous clastic input on the results (Latimer and Filippelli, 2002; Algeo et al., 2011; Zhang X. et al., 2021). The average P/Ti ratio >0.01 indicate high productivity of the lake and it increases with increasing paleoproductivity (Dean et al., 1997; Li et al., 2017). The

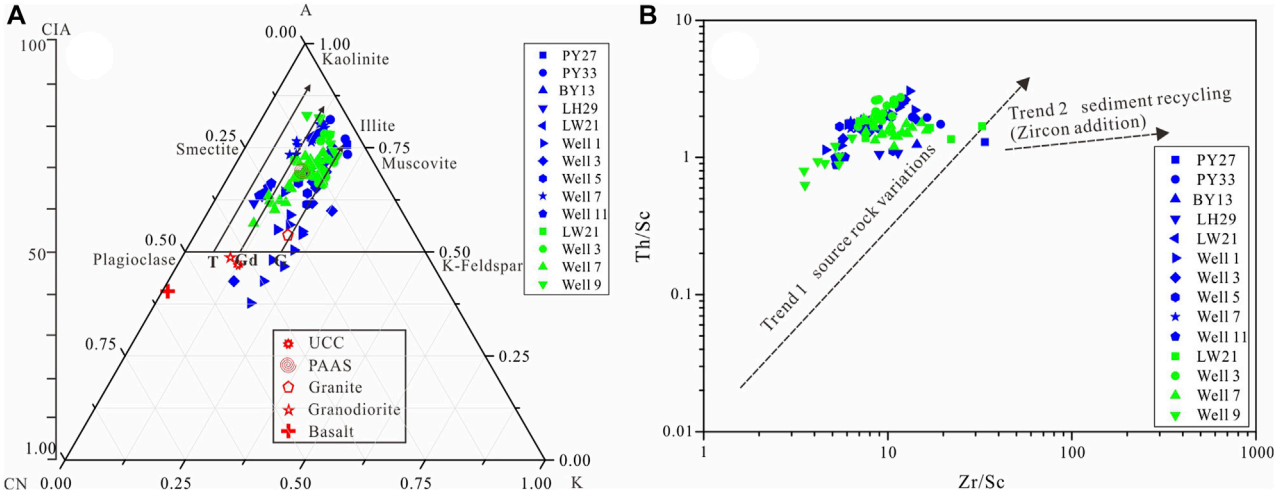

FIGURE 14
(A) A-CN-K (Al_2O_3-CaO*+Na_2O-K_2O) ternary diagram, after Nesbitt and Young (1982). In triangles, three arrowed solid lines parallel to A-CN sidelines are ideal weathering trends of T, Tonalite; Gd, Granodiorite; and G, Granite (Condie, 1993; Xin et al., 2021); **(B)** Zr/Sc vs. Th/Sc diagram for the metasedimentary rocks of this study (McLennan et al., 2003). Th/Sc > 0.79 (solid-line) reflects provenance of samples from the upper continental crust.

P/Ti values of the Wenchang and Enping samples are 0.0418–0.1559 (avg. 0.0933) and 0.028–0.3768 (avg. 0.1011), respectively, indicating high paleoproductivity (S1). Overall, the Ba and P concentrations of the samples indicate that the paleoproductivities of source rocks in both the Wenchang and Enping formations are medium to high.

5.6 Terrigenous clastic input

Al, Zr and Ti are highly resistant accessory elements and less sensitive to weathering or diagenetic processes (Murphy et al., 2000; Calvert and Pedersen, 2007; Ross and Bustin, 2009; Wei and Algeo, 2020b). They are useful indicators of detrital influx (Zhang L. et al., 2021; Li et al., 2021; Song et al., 2021; Xin et al., 2021). Besides, Th/Al is a key indicator to reveal the intensity of terrigenous clastic input. The Ti, Zr and Al_2O_3 profiles for Well 3 show similar patterns, with a relatively stable trend that is associated with the chemical weathering intensity or water depth (Figure 5). Detrital proxies of the samples from Well 7 suggest that the terrigenous flux varies significantly from the Wenchang formation to the Enping formation and increases upward (Figure 6).

5.7 Evolution of depositional environment and organic matter enrichment model

Three organic matter enrichment models have been recognized, namely, the preservation model, production model, and production-preservation co-action model (Calvert and Fontugne, 2001; Mort et al., 2007; Zhu et al., 2022). Cd/Mo and Co×Mn are proposed as effective proxies to distinguish upwelling and hydrographic restricted settings (Sweere et al., 2016; Wu et al., 2022; Zhu et al., 2022). Generally, sediments in upwelling systems are characterized by Mn and Co depletion, while sediments in restricted basins show elevating Mn and Co values (Sweere et al., 2016). The principle of the Cd/Mo proxy lies in the different behaviors of Cd and Mo in seawater. Cd has a close link to primary productivity and displays a nutrient-like profile in water column while Mo behaves conservatively (Conway and John, 2015; Zhu et al., 2022). Thus, low Co×Mn (<0.4) or low Mn_{EF}×Co_{EF} (<0.5) are typical for coastal upwelling settings, while high Co×Mn (>0.4) and high Co_{EF}×Mn_{EF} (>2) for restricted settings like the Black Sea (Zhu et al., 2022). The Co×Mn values of the Wenchang and Enping samples cover a wide range (0.07–8.13, avg. 0.94), with the average higher than 0.4 (Figure 15B). According to the Co*Mn–Cd/Mo plot (Figure 15B), the samples in this study were formed in restricted water conditions, and their organic matter enrichment was mainly controlled by preservation conditions.

Climate during the deposition phase can influence the lake water environment (i.e., depth, salinity, stratification, and aquatic biomass), and the evolution of depositional environment controls the input, deposition and preservation of organic matters (Meng et al., 2012; Li et al., 2016; Shen et al., 2017; Li L. et al., 2019, 2021; Zhang et al., 2020; Xin et al., 2021; Hou et al., 2022). According to the geochemical analyses, the Eocene strata in the Baiyun sag were deposited in a semi-arid to semi-humid climate and oxic–suboxic fresh water environment with relatively large detrital input and stable water depth. During the deposition of the Wenchang and Enping formations, the Baiyun sag mainly developed braided river deltas, beach bars and fan deltas (Zeng et al., 2019). Apparently, the Wenchang formation has a relatively low salinity compared to the Enping formation, and considerable variations from fresh water to brackish in the Enping formation (Figure 5, Figure 6). A closed water system existed during the deposition of the Wenchang formation, and the sea level rose during the deposition of the Enping formation, making the seawater flow over the Liwan sag to the Baiyun sag. The restricted basin was more connected with the ocean and evolved into a semi-restricted basin. Brackish water may cause water stratification and produce a strongly anoxic environment with excellent preservation conditions. Therefore, it is believed that

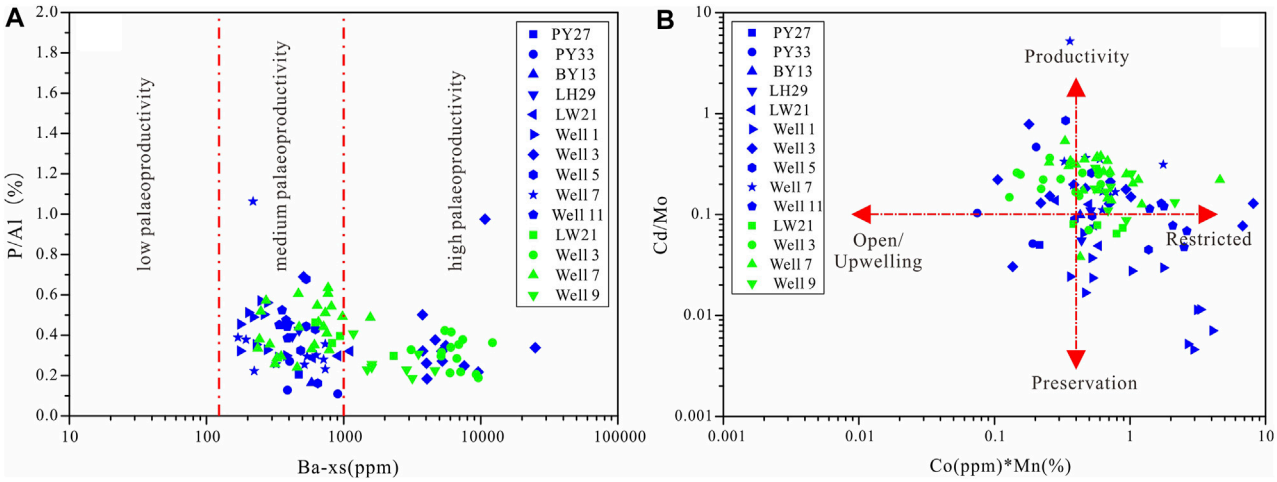

FIGURE 15
(A) Plots of Ba-xs (ppm) vs. P/Al (%) of the mudstone samples in the Bayun Sag; **(B)** Co*Mn–Cd/Mo joint chart. The position of the lines is roughly the boundaries amongst various settings (adopted from Sweere et al., 2016).

both primary productivity and preservation conditions played essential roles in controlling the enrichment of organic matters in the Baiyun sag, and the latter was resulted from the restricted water setting.

6 Conclusion

The paleoenvironment of the Eocene mudstones in the Baiyun sag of the Pearl River Mouth Basin was reconstructed through geochemistry analysis. The conclusions that are obtained as follows:

1) The concentrations and ratios of redox-sensitive trace elements (e.g. U/Th-(Cu+Mo)/Zn, U/Th-V/(V+Ni), U/Th-V/Cr, U/Th-Ni/Co, Ni/Co-V/Cr, Ni/Co-Mo and U_{EF}-Mo_{EF}) reveal that oxic to suboxic conditions were prevailing in the Baiyun sag during the deposition of the Eocene, which is evidenced by biomarkers (e.g. Pr/Ph ratios). The Pr/n-C17–Ph/n-C18 plot indicates that the Eocene strata in the Baiyuan sag were deposited under oxic conditions, with terrigenous organic matters as the major contributor.
2) According to the indices of Sr/Ba, Rb/K, B/Ga and equivalent boron, and the Sr/Ba–Rb/K and V/Ni–Sr/Ba plots, the Eocene strata in the Baiyuan sag were deposited in fresh water to brackish water environment, with increasing salinity from bottom to top. In addition, $\delta^{13}C$ and $\delta^{18}O$ values of carbonate cement for the Enping samples suggest fresh–brackish water lacustrine facies.
3) Representative climate-sensitive major and trace element indices (Sr/Cu, Rb/Sr, C-value, Al_2O_3+K_2O+Na_2O-SiO_2, K_2O/Al_2O_3-Ga/Rb) imply that the mudstones in the Baiyun sag were deposited in semi-arid/warm climate.
4) The Eocene mudstones in the Baiyun sag undergone mild to moderate chemical weathering, which is verified by the CIA, CIW, and PIA indices and the A-CN-K diagram. The study area is believed to have been slightly affected by sedimentary recycling.
5) Both primary productivity and preservation conditions played essential roles in controlling the enrichment of organic matters in the Baiyun sag, and the latter was resulted from the restricted water setting.

Data availability statement

The original contributions presented in the study are included in the article/supplementary material, further inquiries can be directed to the corresponding author.

Author contributions

MM resources, conceptualization, methodology, data curation, formal analysis, writing-review and editing, project administration, funding acquisition. CL investigation, supervision, software, funding acquisition. MR reviewing and editing. All authors contributed to the article and approved the submitted version.

Funding

This work is supported by the Open Funds for Hubei Key Laboratory of Marine Geological Resources, China University of Geosciences (No. MGR202208), the National Natural Science Foundation of China (Grants 42202193) and the Natural Science Foundation of Gansu Province (Grants 22JR5RA080).

Conflict of interest

The authors declare that the research was conducted in the absence of any commercial or financial relationships that could be construed as a potential conflict of interest.

Publisher's note

References

Algeo, T. J., Kuwahara, K., Sano, H., Bates, S., Lyons, T., Elswick, E., et al. (2011). Spatial variation in sediment fluxes, redox conditions, and productivity in the Permian–Triassic Panthalassic Ocean. *Palaeogeogr. Palaeoclimatol. Palaeoecol.* 308, 65–83. doi:10.1016/j.palaeo.2010.07.007

Algeo, T. J., and Li, C. (2020). Redox classification and calibration of redox thresholds in sedimentary systems. *Geochim. Cosmochim. Acta* 287, 8–26. doi:10.1016/j.gca.2020.01.055

Algeo, T. J., and Maynard, J. B. (2004). Trace-element behavior and redox facies in core shales of Upper Pennsylvanian Kansas-type cyclothems. *Chem. Geol.* 206, 289–318. doi:10.1016/j.chemgeo.2003.12.009

Algeo, T. J., and Rowe, H. (2012). Paleoceanographic applications of trace-metal concentration data. *Chem. Geol.* 324, 6–18. doi:10.1016/j.chemgeo.2011.09.002

Algeo, T. J., and Tribovillard, N. (2009). Environmental analysis of paleoceanographic systems based on molybdenum–uranium covariation. *Chem. Geol.* 268, 211–225. doi:10.1016/j.chemgeo.2009.09.001

Arthur, M. A., and Sageman, B. B. (1994). Marine black shales: Depositional mechanisms and environments of ancient deposits. *Annu. Rev. Earth Planet Sci.* 22 (1), 499–551. doi:10.1146/annurev.ea.22.050194.002435

Awan, R. S., Liu, C., Gong, H., Dun, C., Tong, C., and Chamssidini, L. G. (2020). Paleosedimentary environment in relation to enrichment of organic matter of Early Cambrian black rocks of Niutitang Formation from Xiangxi area China. *Mar. Petrol. Geol.* 112, 104057. doi:10.1016/j.marpetgeo.2019.104057

Bai, Y., Liu, Z., Sun, P., Liu, R., Hu, X., Zhao, H., et al. (2015). Rare Earth and major element geochemistry of Eocene fine-grained sediments in oil shale- and coal-bearing layers of the Meihe Basin, northeast China. *J. Asian Earth Sci.* 97, 89–101. doi:10.1016/j.jseaes.2014.10.008

Bennett, W. W., Canfield, D. E., Pre-proof, J., and Bennett, W. W. (2020). Redox-sensitive trace metals as paleoredox proxies: A review and analysis of data from modern sediments. *Earth Sci. Rev.* 204, 103175. doi:10.1016/j.earscirev.2020.103175

Boynton, W. V. (1984). "Geochemistry of the rare Earth elements: Meteorite studies," in *Rare earth element geochemistry*. Editor P. Henderson (Netherlands: Elsevier), 63–114.

Calvert, S. E., and Fontugne, M. R. (2001). On the late Pleistocene-Holocene sapropel record of climatic and oceanographic variability in the eastern Mediterranean. *Paleoceanography* 16, 78–94. doi:10.1029/1999pa000488

Calvert, S. E., and Pedersen, T. F. (2007). Chapter fourteen elemental proxies for palaeoclimatic and palaeoceanographic variability in marine sediments: Interpretation and application. *Dev. Mar. Geol.* 1, 567–644. doi:10.1016/s1572-5480(07)01019-6

Calvert, S. E., and Pedersen, T. F. (1993). Geochemistry of recent oxic and anoxic marine sediments: Implications for the geological record. *Mar. Geol.* 113 (1), 67–88. doi:10.1016/0025-3227(93)90150-t

Cao, J., Wu, M., Chen, Y., Hu, K., Bian, L. Z., Wang, L. G., et al. (2012). Trace and rare Earth element geochemistry of Jurassic mudstones in the northern Qaidam Basin, northwest China. *Chem. Erde – Geochem* 72, 245–252. doi:10.1016/j.chemer.2011.12.002

Cao, L., Zhang, Z., Zhao, J., Jin, X., Li, H., Li, J., et al. (2021). Discussion on the applicability of Th/U ratio for evaluating the paleoredox conditions of lacustrine basins. *Int. J. Coal Geol.* 248, 103868. doi:10.1016/j.coal.2021.103868

Chen, C., Mu, C. L., Zhou, K. K., Liang, W., Ge, X. Y., Wang, X. P., et al. (2016). The geochemical characteristics and factors controlling the organic matter accumulation of the Late Ordovician-Early Silurian black shale in the Upper Yangtze Basin, South China. *Mar. Petrol. Geol.* 76, 159–175. doi:10.1016/j.marpetgeo.2016.04.022

Chen, J., Wang, Y. J., Chen, Y., Liu, L. W., Ji, J. F., and Lu, H. Y. (2001). Geochemical characteristics of Rb and Sr in Chinese Loess and their paleomonsoon climatic significance. *Acta Geol. Sin.* 75 (2), 259–266. (in Chinese with English abstract). doi:10.3321/j.issn:0001-5717.2001.02.016

Chen, S., Qiao, P., Zhang, H., Xie, X., Cui, Y., and Shao, L. (2018). Geochemical characteristics of Oligocene-Miocene sediments from the deepwater area of the northern South China Sea and their provenance implications. *Acta Oceanol. Sin.* 37, 35–43. doi:10.1007/s13131-017-1127-7

Chen, W. T., Du, J. Y., Shi, H. S., and He, M. (2015). Compound hydrocarbon accumulation and enrichment in southwestern huizhou sag, Pearl River Mouth basin, south China sea. *Petroleum Explor. Dev.* 42 (2), 215–222. doi:10.1016/s1876-3804(15)30008-2

Chi, G., Liu, B., Hu, K., Yang, J., and He, B. (2021). Geochemical composition of sediments in the Liao River Estuary and implications for provenance and weathering. *Regional Stud. Mar. Sci.* 45, 101833. doi:10.1016/j.rsma.2021.101833

Chi, G., and Liu, B. (2020). Sedimentary source area and paleoenvironmental reconstruction since late Miocene in the southern South China Sea. *Geochemistry* 80 (1), 125567. doi:10.1016/j.chemer.2019.125567

Condie, K. C. (1993). Chemical composition and evolution of the upper continental crust: Contrasting results from surface samples and shales. *Chem. Geol.* 104, 1–37. doi:10.1016/0009-2541(93)90140-e

Cox, R., Lowe, D. R., and Cullers, R. L. (1995). The influence of sediment recycling and basement composition on evolution of mudrock chemistry in the southwestern United States. *Geochim. Cosmochim. Acta* 59, 2919–2940. doi:10.1016/0016-7037(95)00185-9

Dai, J., Zou, C., Li, J., Ni, Y. Y., Hu, G. Y., Zhang, X. B., et al. (2009). Carbon isotopes of Middle-Lower Jurassic coal-derived alkane gases from the major basins of northwestern China. *Int. J. Coal Geol.* 80, 124–134. doi:10.1016/j.coal.2009.08.007

Dean, W. E., Gardner, J. V., and Piper, D. Z. (1997). Inorganic geochemical indicators of glacialinterglacial changes in productivity and anoxia on the California continental margin. *Geochim. Cosmochim. Acta* 61, 4507–4518. doi:10.1016/s0016-7037(97)00237-8

Degens, E. T., and Ross, D. A. (1974). *The black sea-geology, chemistry, and biology*. Tulsa: The American Association of Petroleum Geologists.

Deininger, M., Fohlmeister, J., Scholz, D., and Mangini, A. (2012). Isotope disequilibrium effects: The influence of evaporation and ventilation effects on the carbon and oxygen isotope composition of speleothems–a model approach. *Geochim. Cosmochim. Acta* 96, 57–79. doi:10.1016/j.gca.2012.08.013

Deng, T., Li, Y., Wang, Z., Yu, Q., Dong, S., Yan, L., et al. (2019). Geochemical characteristics and organic matter enrichment mechanism of black shale in the Upper Triassic Xujiahe Formation in the Sichuan basin: Implications for paleoweathering, provenance and tectonic setting. *Mar. Petroleum Geol.* 109, 698–716. doi:10.1016/j.marpetgeo.2019.06.057

El-Bialy, M. Z. (2013). Geochemistry of the Neoproterozoic metasediments of Malhaq and Um Zariq formations, Kid metamorphic complex, Sinai, Egypt: Implications for source-area weathering, provenance, recycling, and depositional tectonic setting. *Lithos* 175, 68–85. doi:10.1016/j.lithos.2013.05.002

Fedo, C. M., Nesbitt, H. W., and Young, G. M. (1995). Unraveling the effects of potassium metasomatism in sedimentary rocks and paleosols, with implications for paleoweathering conditions and provenance. *Geology* 23, 921–924. doi:10.1130/0091-7613(1995)023<0921:uteopm>2.3.co;2

Feng, R., and Kerrich, R. (1990). Geochemistry of fine-grained clastic sediments in the Archean Abitibi greenstone belt, Canada: Implications for provenance and tectonic setting. *Geochim. Cosmochim. Acta* 54, 1061–1081. doi:10.1016/0016-7037(90)90439-r

Fu, J., Chen, C., Li, M., Zhang, Z., Long, Z., Wang, T., et al. (2020). Petroleum charging history of neogene reservoir in the Baiyun sag, Pearl River Mouth Basin, south China sea. *J. Petroleum Sci. Eng.* 190, 106945. doi:10.1016/j.petrol.2020.106945

Fu, J., Zhang, Z., Chen, C., Wang, T. G., Li, M., Ali, S., et al. (2019). Geochemistry and origins of petroleum in the neogene reservoirs of the Baiyun sag, Pearl River Mouth basin. *Mar. Petroleum Geol.* 107, 127–141. doi:10.1016/j.marpetgeo.2019.05.015

Fu, X. G., Wang, J., Chen, W. B., Feng, X. L., Wang, D., Song, C. Y., et al. (2016). Elemental geochemistry of the early jurassic black shales in the qiangtang basin, eastern tethys: Constraints for palaeoenvironment conditions. *Geol. J.* 51, 443–454. doi:10.1002/gj.2642

Gao, S., and Wedepohl, K. H. (1995). The negative Eu anomaly in archean sedimentary rocks: Implications for decomposition, age and importance of their granitic sources. *Earth Planet. Sci. Lett.* 133, 81–94. doi:10.1016/0012-821x(95)00077-p

González, P. A. A., Garban, G., Hauser, N., and Gigena, L. (2017). Geochemistry of metasedimentary rocks from the puncoviscana complex in the mojotoro range, NW Argentina: Implications for provenance and tectonic setting. *J. S. Am. Earth Sci.* 78, 250–263. doi:10.1016/j.jsames.2017.06.003

Götze, J. (1998). Geochemistry and provenance of the altendorf feldspathicsandstone in the middle bunter of the thuringian basin, Germany. *Chem. Geol.* 150, 43–61. doi:10.1016/s0009-2541(98)00052-7

Guo, H. L., and Wang, D. R. (1999). Tarim expected the isotopic composition of sandstone reservoir in carbonate cements and cause analysis[J]. *Petroleum Explor. Dev.* 26 (3), 31–32. (in Chinese with English abstract).

Hakimi, M. H., Abdullah, W. H., and Shalaby, M. R. (2011). Organic geochemical characteristics and depositional environments of the Jurassic shales in the Masila basin of Eastern Yemen. *GeoArabia* 16, 47–64. doi:10.2113/geoarabia160147

Hallberg, R. O. A. (1976). Geochemical method for investigation of paleoredox conditions in sediments. *Ambio Spec. Rep.* 4, 139–147.

Harnois, L. (1988). The CIW index: A new chemical index of weathering. *Sediment. Geol.* 55, 319–322. doi:10.1016/0037-0738(88)90137-6

Hatch, J. R., and Leventhal, J. S. (1992). Relationship between inferred redox potential of the depositional environment and geochemistry of the Upper Pennsylvanian (Missourian) Stark shale member of the dennis limestone, Wabaunsee County, Kansas, USA. *Chem. Geol.* 99 (1/2/3), 65–82. doi:10.1016/0009-2541(92)90031-y

He, C., Ji, L., Wu, Y. D., Su, A., and Zhang, M. Z. (2016). Characteristics of hydrothermal sedimentation process in the yanchang formation, south ordos basin, China: Evidence from element geochemistry. *Sediment. Geol.* 345, 33–41. doi:10.1016/j.sedgeo.2016.09.001

He, D., Hou, D., and Chen, T. (2018). Geochemical characteristics and analysis of crude-oil source in the deep-water area of the Baiyun Sag, South China Sea. *Russ. Geol. Geophys.* 59 (5), 499–511. doi:10.1016/j.rgg.2018.04.004

He, J., Garzanti, E., Cao, L., and Wang, H. (2020). The zircon story of the Pearl River (China) from Cretaceous to present. *Earth-Science Rev.* 201, 103078. doi:10.1016/j.earscirev.2019.103078

Herron, M. M. (1988). Geochemical classification of terrigenous sands and shales from core or log data. *J. Sediment. Petrol.* 58, 820–829.

Holland, H. D. (1978). *The chemistry of the atmosphere and oceans*. New York: Wiley-Interscience.

Hou, H., Shao, L., Li, Y., Liu, L., Liang, G., Zhang, W., et al. (2022). Effect of paleoclimate and paleoenvironment on organic matter accumulation in lacustrine shale: Constraints from lithofacies and element geochemistry in the northern Qaidam Basin, NW China. *J. Petroleum Sci. Eng.* 208, 109350. doi:10.1016/j.petrol.2021.109350

Jia, J., Bechtel, A., Liu, Z., Susanne, A. I., Strobl, P. S., and Reinhard, F. S. (2013a). Oil shale formation in the Upper cretaceous Nenjiang formation of the Songliao Basin (NE China): Implications from organic and inorganic geochemical analyses. *Int. J. Coal Geol.* 113, 11–26. doi:10.1016/j.coal.2013.03.004

Jia, J., Liu, Z., Bechtel, A., Strobl, Susanne A. I., and Sun, P. (2013b). Tectonic and climate control of oil shale deposition in the upper cretaceous qingshankou formation (songliao basin, NE China). *Int. J. Earth Sci.* 102 (6), 1717–1734. doi:10.1007/s00531-013-0903-7

Jiang, W., Chen, C., Long, Z., Li, Y., Yang, C., and Xiong, Y. (2022). Geochemical characteristics and possible sources of crude oils in the Baiyun deep-water area of the Pearl River Mouth basin, south China sea. *Mar. Petroleum Geol.* 135, 105410. doi:10.1016/j.marpetgeo.2021.105410

Jones, B., and Manning, D. (1994). Comparison of geochemical indices used for the interpretation of palaeoredox conditions in ancient mudstones. *Chem. Geol.* 111, 111–129. doi:10.1016/0009-2541(94)90085-x

Keith, M. L., and Weber, J. N. (1964). Carbon and oxygen isotopic composition of selected limestones and fossils. *Geochem. Cosmochim. Acta* 28 (S1), 1787–1816. doi:10.1016/0016-7037(64)90022-5

Kimura, H., and Watanabe, Y. (2001). Oceanic anoxia at the Precambrian-Cambrian boundary. *Geology* 29 (11), 995. doi:10.1130/0091-7613(2001)029<0995:oaatpc>2.0.co;2

Kong, L., Chen, H., Ping, H., Zhai, P., Liu, Y., and Zhu, J. (2018). Formation pressure modeling in the Baiyun Sag, northern South China Sea: Implications for petroleum exploration in deep-water areas. *Mar. Petroleum Geol.* 97, 154–168. doi:10.1016/j.marpetgeo.2018.07.004

Langmuir, D. (1978). Uranium solution-mineral equilibria at low temperatures with applications to sedimentary ore deposits. *Geochimica Cosmochimica Acta* 42, 547–569. doi:10.1016/0016-7037(78)90001-7

Latimer, J. C., and Filippelli, G. M. (2002). Eocene to miocene terrigenous inputs and export production: Geochemical evidence from ODP leg 177, site 1090. *Paleogeogr. Paleoclimatol. Paleoecol.* 182, 151–164. doi:10.1016/s0031-0182(01)00493-x

Lerman, A. (1978). *Lakes: Chemistry, geology, physics*. Germany: Springer Press, Verlag Berlin Heidelberg, 10–100.

Li, D., Li, R., Zhu, Z., Wu, X., Cheng, J., Liu, F., et al. (2017). Origin of organic matter and paleo-sedimentary environment reconstruction of the Triassic oil shale in Tongchuan City, southern Ordos Basin (China). *Fuel* 208, 223–235. doi:10.1016/j.fuel.2017.07.008

Li, L., Liu, Z., George, S. C., Sun, P., Xu, Y., Meng, Q., et al. (2019a). Lake evolution and its influence on the formation of oil shales in the middle jurassic shimengou Formation in the tuanyushan area, qaidam basin, NW China. *Geochemistry* 79 (1), 162–177. doi:10.1016/j.geoch.2018.12.006

Li, M., Shao, L. Y., Liu, L., Lu, J., Spiro, B., Wen, H. J., et al. (2016). Lacustrine basin evolution and coal accumulation of the Middle Jurassic in the Saishiteng coalfield, northern Qaidam Basin, China. *J. Palaeogeogr.* 5 (3), 205–220. doi:10.1016/j.jop.2016.03.001

Li, Y., Jiang, Z., Liu, H., Shi, C., Huang, Y., and Zhang, H. (2020). Using element geochemistry and detrital zircon geochronology to constrain provenance of the Eocene sediments in the deep-water area of the Pearl River Mouth Basin, South China Sea. *J. Asian Earth Sci.* 204, 104501. doi:10.1016/j.jseaes.2020.104501

Li, Y., Sun, P., Liu, Z., Xu, Y., Liu, R., and Ma, L. (2021). Factors controlling the distribution of oil shale layers in the Eocene Fushun Basin, NE China. *Mar. Petroleum Geol.* 134, 105350. doi:10.1016/j.marpetgeo.2021.105350

Li, Y., Wang, Z., Gan, Q., Niu, X., and Xu, W. (2019b). Paleoenvironmental conditions and organic matter accumulation in Upper Paleozoic organic-rich rocks in the east margin of the Ordos Basin, China. *Fuel* 252, 172–187. doi:10.1016/j.fuel.2019.04.095

Lin, C., He, M., Steel, R. J., Zhang, Z., Li, H., Zhang, B., et al. (2018). Changes in inner- to outer-shelf delta architecture, Oligocene to Quaternary Pearl River shelf-margin prism, northern South China Sea. *Mar. Geol.* 404, 187–204. doi:10.1016/j.margeo.2018.07.009

Liu, B., Song, Y., Zhu, K., Su, P., Ye, X., and Zhao, W. (2020). Mineralogy and element geochemistry of salinized lacustrine organic-rich shale in the Middle Permian Santanghu Basin: Implications for paleoenvironment, provenance, tectonic setting and shale oil potential. *Mar. Petroleum Geol.* 120, 104569. doi:10.1016/j.marpetgeo.2020.104569

Liu, J., Zheng, R. C., Gou, X. F., Wang, C. Y., Deng, G., Xu, X., et al. (2015). C5aR, TNF-α, and FGL2 contribute to coagulation and complement activation in virus-induced fulminant hepatitis. *J. Chengdu Univ. Technol. Sci. Technol. Ed.* 42 (3), 354–362. (in Chinese with English abstract). doi:10.1016/j.jhep.2014.08.050

Liu, S., Liu, B., Tang, S., Zhao, C., Tan, F., Xi, Z., et al. (2022). Palaeoenvironmental and tectonic controls on organic matter enrichment in the middle jurassic dameigou formation (qaidam basin, north China). *Palaeogeogr. Palaeoclimatol. Palaeoecol.* 585, 110747. doi:10.1016/j.palaeo.2021.110747

Ma, M., Chen, G., Li, C., Zhang, G., Lv, C., Xue, L., et al. (2019). Petrography and geochemistry of Oligocene to lower miocene sandstones in the Baiyun sag, Pearl River Mouth basin, south China sea: Provenance, source area weathering, and tectonic setting. *Geol. J.* 54 (1), 564–589. doi:10.1002/gj.3207

Ma, M., Chen, G., Zhang, G., Rahman, M. J. J., and Ma, X. (2022). Geochemistry and provenance of Oligocene to middle miocene sandstones in the qiongdongnan basin, northern South China sea. *Mar. Geol.* 447, 106794. doi:10.1016/j.margeo.2022.106794

Ma, M., Li, C., Lu, C., Chen, G., Yang, F., Yan, Y., et al. (2017). Geochemistry and provenance of a multiple-stage fan in the upper miocene to the pliocene in the yinggehai and qiongdongnan basins, offshore south China sea. *Mar. Pet. Geol.* 79, 64–80. doi:10.1016/j.marpetgeo.2016.11.001

Ma, Y. Q., Fan, M. J., Lu, Y. C., Liu, H. M., Hao, Y. Q., Xie, Z. H., et al. (2016). Climate-driven paleolimnological change controls lacustrine mudstone depositional process and organic matter accumulation: Constraints from lithofacies and geochemical studies in the Zhanhua Depression, eastern China. *Int. J. Coal Geol.* 167, 103–118. doi:10.1016/j.coal.2016.09.014

Madhavaraju, J., Ramírez-Montoya, E., Monreal, R., González-León, C. M., Pi-Puig, T., Espinoza-Maldonado, I. G., et al. (2016). Paleoclimate, paleoweathering and paleoredox conditions of lower cretaceous shales from the mural limestone, tuape section, northern sonora, Mexico: Constraints from clay mineralogy and geochemistry. *Rev. Mex. Ciencias Geol.* 33 (1), 34–48.

Makeen, Y. M., Abdullah, W. H., Ayinla, H. A., Shan, X., Liang, Y., Su, S., et al. (2019). Organic geochemical characteristics and depositional setting of Paleogene oil shale, mudstone and sandstone from onshore Penyu Basin, Chenor, Pahang, Malaysia. *Int. J. Coal Geol.* 207, 52–72. doi:10.1016/j.coal.2019.03.012

Mclennan, S. M., Bock, B., Hemming, S. R., Hurowitz, J. A., Steven, M. L., and Mcdaniel, D. K. (2003). "The roles of provenance and sedimentary processes in the geochemistry of sedimentary rocks," in *Geochemistry of sediments and sedimentary rocks/evolutionary considerations to mineral deposit-forming environments*. Editor D. R. Lentz (Canada: Geological Association of Canada), 4, 1–6.

McLennan, S. M., Hemming, D. K., McDaniel, D. K., and Hanson, G. N. (1993). Geochemical approaches to sedimentation, provenance, and tectonics. *Geol. Soc. Am. Spec. Pap.* 284, 21–40.

McLennan, S., Taylor, S., and Kroner, A. (1983). Geochemical evolution of archean shales from south Africa. I: The Swaziland and pongola supergroups. *Precambrian Res.* 22, 93–124. doi:10.1016/0301-9268(83)90060-8

Meng, Q. T., Liu, Z. J., Bruch, A. A., and Liu, R. (2012). Palaeoclimatic evolution during Eocene and its influence on oil shale mineralisation, Fushun basin, China. *J. Asia Earth Sci.* 45, 95–105. doi:10.1016/j.jseaes.2011.09.021

Mi, L. J., Zhang, Z. T., Pang, X., Liu, J., Zhang, B., Zhao, Q., et al. (2018). Main controlling factors of hydrocarbon accumulation in Baiyun Sag at northern continental margin of South China Sea. *Petrol. explor. Dev.* 45 (5), 963–973. doi:10.1016/s1876-3804(18)30100-9

Miao, S. D., Zhang, G. C., Liang, J. S., Yang, H. Z., Ji, M., Shen, H. L., et al. (2013). Delta depositional system and source rock characteristics of Enping Formation, Liwan sag in ultra deep-water area of nothern South China Sea. *ACTA PET. SIN.* 34 (2), 57–65. (in Chinese with English abstract). doi:10.7623/syxb2013S2007

Moradi, A. V., Sari, A., and Akkaya, P. (2016). Geochemistry of the miocene oil shale (hançili formation) in the çankırı-çorum basin, central Turkey: Implications for paleoclimate conditions, source–area weathering, provenance and tectonic setting. *Sediment. Geol.* 341, 289–303. doi:10.1016/j.sedgeo.2016.05.002

Mort, H., Jacquat, O., Adatte, T., Steinmann, P., Föllmi, K., Matera, V., et al. (2007). The cenomanian/turonian anoxic event at the bonarelli level in Italy and Spain: Enhanced productivity and/or better preservation? *Cretac. Res.* 28, 597–612. doi:10.1016/j.cretres.2006.09.003

Murphy, A. E., Sageman, B. B., Hollander, D. J., Lyons, T. W., and Brett, C. E. (2000). Black shale deposition and faunal overturn in the devonian appalachian basin: Clastic starvation, seasonal water–column mixing, and efficient biolimiting nutrient recycling. *Paleoceanography* 15, 280–291. doi:10.1029/1999pa000445

Nesbitt, H. W., and Young, G. M. (1984). Prediction of some weathering trends of plutonic and volcanic rocks based on thermodynamic and kinetic considerations. *Geochim. Cosmochim. Acta* 48 (7), 1523–1534. doi:10.1016/0016-7037(84)90408-3

Nesbitt, H. W., and Young, G. M. (1982). Early Proterozoic climates and plate motions inferred from major element chemistry of lutites. *Nature* 299 (5885), 715–717. doi:10.1038/299715a0

Oyebanjo, O., Ekosse, G. I., and Odiyo, J. (2018). Geochemical characterisation of the< 2 µm fractions of cretaceous-tertiary kaolins from eastern dahomey and Niger delta basins, Nigeria: Implications on paleoenvironment, provenance, and tectonic settings. *J. Afr. Earth Sci.* 147, 402–410. doi:10.1016/j.jafrearsci.2018.07.010

Pan, X., Wang, Z., Li, Q., Gao, J., Zhu, L., and Liu, W. (2020). Sedimentary environments and mechanism of organic matter enrichment of dark shales with low TOC in the Mesoproterozoic Cuizhuang Formation of the Ordos Basin: Evidence from petrology, organic geochemistry, and major and trace elements. *Mar. Petroleum Geol.* 122, 104695. doi:10.1016/j.marpetgeo.2020.104695

Pang, X., Chen, C., Peng, D., Zhu, M., Shu, Y., He, M., et al. (2007). Sequence stratigraphy of deep-water fan system of Pearl River, south China sea. *Earth Sci. Front.* 14 (1), 220–229. doi:10.1016/s1872-5791(07)60010-4

Paytan, A., and Griffith, E. M. (2007). Marine barite: Recorder of variations in ocean export productivity. *Deep-Sea Res. Ii.* 54 (5–7), 687–705. doi:10.1016/j.dsr2.2007.01.007

Perkins, R. B., and Mason, C. E. (2015). The relative mobility of trace elements from short-term weathering of a black shale. *Appl. Geochem.* 56, 67–79. doi:10.1016/j.apgeochem.2015.01.014

Peters, K. E., Walters, C. C., and Moldowan, J. M. (2005). "Biomarker guide: Volume 2," in *Biomarkers and isotopes in petroleum exploration and earth history*. 2nd ed. (Cambridge: Cambridge University Press), 476–971.

Pettijohn, F. J., Potter, P. E., and Siever, R. (1972). *Sand and sandstone*. Berlin: Springer-Verlag.

Pettijohn, F. J., Potter, P. E., and Siever, R. (1987). *Sand and sandstone*. New York: Springer, 553p.

Piper, D. Z., and Perkins, R. B. (2004). A modern vs. Permian black shale—The hydrography, primary productivity, and water-column chemistry of deposition. *Chem. Geol.* 206, 177–197. doi:10.1016/j.chemgeo.2003.12.006

Qadrouh, A. N., Alajmi, M. S., Alotaibi, A. M., Baioumy, H., Alyousif, M. M., Ahmed Salim, A. M., et al. (2021). Mineralogical and geochemical imprints to determine the provenance, depositional environment, and tectonic setting of the Early Silurian source rock of the Qusaiba shale, Saudi Arabia. *Saudi Arab. Mar. Petroleum Geol.* 130, 105131. doi:10.1016/j.marpetgeo.2021.105131

Ross, J. K., and Bustin, R. M. (2009). Investigating the use of sedimentary geochemical proxies for paleoenvironment interpretation of thermally mature organic-rich strata, Examples from the Devonian–Mississippian shales, Western Canadian Sedimentary Basin. *Chem. Geol.* 260, 1–19. doi:10.1016/j.chemgeo.2008.10.027

Roy, D. K., and Roser, B. P. (2013). Climatic control on the composition of Carboniferous-Permian Gondwana sediments, Khalaspir basin, Bangladesh. *Gondwana Res.* 23 (3), 1163–1171. doi:10.1016/j.gr.2012.07.006

Rudnick, R., and Gao, S. (2003). Composition of the continental crust. *Treatise geochem.* 3, 1–64.

Sajid, Z., Ismail, M. S., and Hanif, T. (2020). Mineralogical and geochemical imprints to determine the provenance, depositional history and tectonic settings of Triassic turbidites in the Semanggol and Semantan Basins, Peninsular Malaysia. *J. Asian Earth Sci.* 203, 104539. doi:10.1016/j.jseaes.2020.104539

Shanmugam, G. (1985). Significance of coniferous rain forests and related organic matter in generating commercial quantities of oil. Gippsland Basin, Australia. *AAPG Bull.* 69, 1241–1254.

Shao, L., Cao, L., Pang, X., Jiang, T., Qiao, P., and Zhao, M. (2016). Detrital zircon provenance of the P aleogene syn-rift sediments in the northern S outh C hina S ea. *Geochem. Geophys. Geosystems* 17 (2), 255–269. doi:10.1002/2015gc006113

Shen, Y. L., Qin, Y., Wang, G. G. X., Guo, Y. H., Shen, J., Gu, J. Y., et al. (2017). Sedimentary control on the formation of a multisuperimposed gas system in the development of key layers in the sequence framework. *Mar. Petrol. Geol.* 88, 268–281. doi:10.1016/j.marpetgeo.2017.08.024

Shi, C., Long, Z. L., Zhu, J. Z., Jiang, Z. L., and Huang, Y. P. (2020). Element geochemistry of the Enping Formation in the Baiyun sag of Pearl River Mouth basin and their environmental implications. *Mar. Geol. Quat. Geol.* 40 (5), 79–86. (in Chinese with English abstract). doi:10.16562/j.cnki.0256-1492.2020042101

Shields, G., and Stille, P. (2001). Diagenetic constraints on the use of cerium anomalies as palaeoseawater redox proxies: An isotopic and REE study of cambrian phosphorites. *Chem. Geol.* 175, 29–48. doi:10.1016/s0009-2541(00)00362-4

Song, Y., Cao, Q., Li, S., Hu, S., Zhu, K., Ye, X., et al. (2021). Salinized lacustrine organic-rich shale influenced by marine incursions: Algal-microbial community, paleoenvironment and shale oil potential in the Paleogene Biyang Depression, East China. *Palaeogeogr. Palaeoclimatol. Palaeoecol.* 580, 110621. doi:10.1016/j.palaeo.2021.110621

Song, Y., Liu, Z. J., Sun, P. C., Meng, Q. T., and Liu, R. (2017). A comparative geochemistry study of several oil shale-bearing intervals in the Paleogene Huadian Formation, Huadian Basin, northeast China. *J. Earth Sci.* 28, 645–655. doi:10.1007/s12583-016-0638-z

Sun, P. C., Chsenhofer, R. F., Liu, Z. J., Strobl, S. A. I., Meng, Q. T., Liu, R., et al. (2013). Organic matter accumulation in the oil shale and coal-bearing Huadian Basin (Eocene; NE China). *Int. J. Coal Geol.* 105, 1–15. doi:10.1016/j.coal.2012.11.009

Sun, Q., Wu, S., Cartwright, J., and Dong, D. (2012). Shallow gas and focused fluid flow systems in the Pearl River Mouth basin, northern South China sea. *Mar. Geol.* 315, 1–14. doi:10.1016/j.margeo.2012.05.003

Suttner, L. J., and Dutta, P. K. (1986). Alluvial sandstone composition and palaeoclimate. 1. Framework mineralogy. *J. Sediment. Petrol.* 56, 329–345.

Sweere, T., van den Boorn, S., Dickson, A. J., and Reichart, G.-J. (2016). Definition of new trace-metal proxies for the controls on organic matter enrichment in marine sediments based on Mn, Co, Mo and Cd concentrations. *Chem. Geol.* 441, 235–245. doi:10.1016/j.chemgeo.2016.08.028

Tanaka, K., Akagawa, F., Yamamoto, K., Tani, Y., Kawabe, I., and Kawai, T. (2007). Rare Earth element geochemistry of lake baikal sediment: Its implication for geochemical response to climate change during the last glacial/interglacial transition. *Quat. Sci. Rev.* 26, 1362–1368. doi:10.1016/j.quascirev.2007.02.004

Tao, S., Xu, Y., Tang, D., Xu, H., Li, S., Chen, S., et al. (2017). Geochemistry of the Shitoumei oil shale in the Santanghu Basin, Northwest China: Implications for paleoclimate conditions, weathering, provenance and tectonic setting. *Int. J. Coal Geol.* 184, 42–56. doi:10.1016/j.coal.2017.11.007

Taylor, S. R., and McLennan, S. M. (1985). *The continental crust: Its composition and evolution*. Oxford: Blackwell Scientific Publishers.

Tribovillard, N., Algeo, T. J., Lyons, T., and Riboulleau, A. (2006). Trace metals as paleoredox and paleoproductivity proxies: An update. *Chem. Geol.* 232, 12–32. doi:10.1016/j.chemgeo.2006.02.012

Tyrrell, T. (1999). The relative influences of nitrogen and phosphorus on oceanic primary production. *Nature* 400 (6744), 525–531. doi:10.1038/22941

Van de Kamp, P. C., and Leake, B. E. (1985). Petrography and geochemistry of feldspathic and mafic sediments of the northeastern pacific margin. *Transaction R. Soc. Edinb. Earth Sci.* 76, 411–449. doi:10.1017/s0263593300010646

Vincent, B., Rambeau, C., Emmanuel, L., and Loreau, J. P. (2006). Sedimentology and trace element geochemistry of shallow-marine carbonates: An approach to paleoenvironmental analysis along the pagny-sur-meuse section (upper jurassic, France). *Facies* 52 (1), 69–84. doi:10.1007/s10347-005-0026-0

Walker, C. T. (1968). Evaluation of boron as a paleosalinity indicator and its application to offshore prospects. *AAPG Bull.* 52 (5), 751–766.

Wang, C., Zeng, J., Zhang, Z., Shi, N., Lao, M., Zhao, Q., et al. (2018a). Origin and distribution of natural gas and oil in the Baiyun depression, Pearl River Mouth Basin, south China sea. *J. Petroleum Sci. Eng.* 170, 467–475. doi:10.1016/j.petrol.2018.06.056

Wang, W., Yang, X., Bidgoli, T. S., and Ye, J. (2019). Detrital zircon geochronology reveals source-to-sink relationships in the Pearl River Mouth Basin, China. *Sediment. Geol.* 388, 81–98. doi:10.1016/j.sedgeo.2019.04.004

Wang, Z., Wang, J., Fu, X., Zhan, W., Armstrong-Altrin, J. S., Yu, F., et al. (2018b). Geochemistry of the upper triassic black mudstones in the qiangtang basin, tibet: Implications for paleoenvironment, provenance, and tectonic setting. *J. Asian Earth Sci.* 160, 118–135. doi:10.1016/j.jseaes.2018.04.022

Wei, W., and Algeo, T. J. (2020a). Elemental proxies for paleosalinity analysis of ancient shales and mudrocks. *Geochim. Cosmochim. Acta* 287, 341–366. doi:10.1016/j.gca.2019.06.034

Wei, W., Algeo, T. J., Lu, Y. B., Lu, Y. C., Liu, H.,M., Zhang, S. P., et al. (2018). Identifying marine incursions into the Paleogene Bohai Bay Basin lake system in northeastern China. *Int. J. Coal Geol.* 200, 1–17. doi:10.1016/j.coal.2018.10.001

Wei, W., and Algeo, T. J. (2020b). Secular variation in the elemental composition of marine shales since 840 Ma: Tectonic and seawater influences. *Geochim. Cosmochim. Acta* 287, 367–390. doi:10.1016/j.gca.2020.01.033

Wignall, P. B., and Twitchett, R. J. (1996). Oceanic anoxia and the end permian mass extinction. *Science* 5265 (272), 1155–1158. doi:10.1126/science.272.5265.1155

Worash, G. (2002). Geochemistry provenance and depositional tectonic setting of the Adigrat Sandstone northern Ethiopia. *J. Afr. Earth Sci.* 35, 185–198. doi:10.1016/s0899-5362(02)00126-4

Wu, Y., Liu, C., Liu, Y., Gong, H., Awan, R. S., Li, G., et al. (2022). Geochemical characteristics and the organic matter enrichment of the upper ordovician tanjianshan group, qaidam basin, China. *J. Petroleum Sci. Eng.* 208, 109383. doi:10.1016/j.petrol.2021.109383

Xi, D. P., Wan, X. Q., Jansa, L., and Zhang, Y. Y. (2011). Late Cretaceous paleoenvironment and lake level fluctuation in the Songliao Basin, northeastern China. *Isl. Arc* 20, 6–22. doi:10.1111/j.1440-1738.2010.00753.x

Xie, H., Zhou, D., Li, Y. P., Pang, X., Li, P. C., Chen, G. H., et al. (2014). Cenozoic tectonic subsidence in deepwater sags in the Pearl River Mouth basin, northern South China sea. *Tectonophysics* 615-616, 182–198. doi:10.1016/j.tecto.2014.01.010

Xie, W., Tan, J., Wang, W., Schulz, H. M., Liu, Z., Kang, X., et al. (2021). Middle jurassic lacustrine source rocks controlled by an aridification event: A case study in the northern qaidam basin (NW China). *Int. J. Coal Geol.* 242, 103779. doi:10.1016/j.coal.2021.103779

Xin, B., Hao, F., Han, W., Xu, Q., Zhang, B., and Tian, J. (2021). Paleoenvironment evolution of the lacustrine organic-rich shales in the second member of Kongdian Formation of Cangdong Sag, Bohai Bay Basin, China: Implications for organic matter accumulation. *Mar. Petroleum Geol.* 133, 105244. doi:10.1016/j.marpetgeo.2021.105244

Xu, S. C., Liu, Z. J., Zhang, P., Boak, J. M., Liu, R., and Meng, Q. T. (2016). Characterization of depositional conditions for lacustrine oil shales in the eocene jijuntun formation, fushun basin, NE China. *Int. J. Coal Geol.* 167, 10–30. doi:10.1016/j.coal.2016.09.004

Xu, X., Xu, S., Liu, J., Chen, L., Liang, H., Mei, L., et al. (2021). Thermal maturation, hydrocarbon generation and expulsion modeling of the source rocks in the Baiyun sag, Pearl River Mouth basin, south China sea. *J. Petroleum Sci. Eng.* 205, 108781. doi:10.1016/j.petrol.2021.108781

Yan, D., Li, S., Fu, H., Jasper, D. M., Zhou, S., Yang, X., et al. (2021). Mineralogy and geochemistry of lower silurian black shales from the yangtze platform, south China. *Int. J. Coal Geol.* 237, 103706. doi:10.1016/j.coal.2021.103706

Yan, L. J., and Zheng, M. P. (2015). The response of lake variations to climate change in the past forty years: A case study of the northeastern Tibetan plateau and adjacent areas, China. *Quat. Int.* 371, 31–48. doi:10.1016/j.quaint.2014.12.057

Yeasmin, R., Chen, D., Fu, Y., Wang, J., Guo, Z., and Guo, C. (2017). Climatic-oceanic forcing on the organic accumulation across the shelf during the early cambrian (age 2 through 3) in the mid-upper yangtze block, NE guizhou, south China. *J. Asian Earth Sci.* 134, 365–386. doi:10.1016/j.jseaes.2016.08.019

Yi, L., Bin, X., Ge, L., Xue, J. C., Xiao, Q. H., Pin, Y., et al. (2007). Geochemistry of the sedimentary rocks from the Nanxiong Basin, South China and implications for provenance, paleoenvironment and paleoclimate at the K/T boundary. Sediment. *Geol* 197, 127–140.

Yuan, L., Jiang, W., Li, Y., and Xiong, Y. (2021). Combining catalytic hydropyrolysis and GC–IRMS to reconstruct the geochemical characteristics of source rocks in the Baiyun deep-water area of the Pearl River Mouth Basin, China. *Mar. Petroleum Geol.* 131, 105166. doi:10.1016/j.marpetgeo.2021.105166

Zaid, S. M. (2015). Geochemistry of sandstones from the pliocene gabir formation, north marsa alam, red sea, Egypt: Implication for provenance, weathering and tectonic setting. *J. Afr. Earth Sci.* 102, 1–17. doi:10.1016/j.jafrearsci.2014.10.016

Zanin, Y. N., Eder, V. G., Zamirailova, Al.G., and Krasavchikov, V. O. (2010). Models of the REE distribution in the black shale Bazhenov Formation of the West Siberian marine basin, Russia. *Chem. der-Erde* 70, 363–376. doi:10.1016/j.chemer.2010.04.001

Zeng, S. Q., Wang, J., Fu, X. G., Chen, W. B., Feng, X. L., Wang, D., et al. (2015). Geochemical characteristics, redox conditions, and organic matter accumulation of marine oil shale from the Changliang Mountain area, northern Tibet. China. *Mar. Pet. Geol.* 64, 203–221. doi:10.1016/j.marpetgeo.2015.02.031

Zeng, Z., Zhu, H., Yang, X., Zeng, H., Xia, C., and Chen, Y. (2019). Using seismic geomorphology and detrital zircon geochronology to constrain provenance evolution and its response of Paleogene Enping Formation in the Baiyun Sag, Pearl River Mouth Basin, South China sea: Implications for paleo-Pearl River drainage evolution. *J. Petroleum Sci. Eng.* 177, 663–680. doi:10.1016/j.petrol.2019.02.051

Zhang, L., Dong, D., Qiu, Z., Wu, C., Zhang, Q., Wang, Y., et al. (2021a). Sedimentology and geochemistry of Carboniferous-Permian marine-continental transitional shales in the eastern Ordos Basin, North China. *Palaeogeogr. Palaeoclimatol. Palaeoecol.* 571, 110389. doi:10.1016/j.palaeo.2021.110389

Zhang, X., Gao, Z., Fan, T., Xue, J., Li, W., Cao, F., et al. (2021b). Geochemical characteristics, provenance and paleodepostional environment of the lower jurassic huxishan Formation in the lenghu area, northwestern qaidam basin, north west China: Implications for organic matter origin. *J. Petroleum Sci. Eng.* 205, 108951. doi:10.1016/j.petrol.2021.108951

Zhang, X., Gao, Z., Fan, T., Xue, J., Li, W., Zhang, H., et al. (2020). Element geochemical characteristics, provenance attributes, and paleosedimentary environment of the Paleogene strata in the Lenghu area, northwestern Qaidam Basin. *J. Petroleum Sci. Eng.* 195, 107750. doi:10.1016/j.petrol.2020.107750

Zhang, X., Lin, C., Zahid, M. A., Jia, X., and Zhang, T. (2017). Paleosalinity and water body type of eocene Pinghu formation, Xihu depression, East China Sea Basin. *J. Petroleum Sci. Eng.* 158, 469–478. doi:10.1016/j.petrol.2017.08.074

Zhao, N., Ye, J., Yang, B., Zhang, F., Yu, H., Xu, C., et al. (2021). Depositional palaeoenvironment and models of the Eocene lacustrine source rocks in the northern South China Sea. *Mar. Petroleum Geol.* 128, 105015. doi:10.1016/j.marpetgeo.2021.105015

Zhao, Y., Ren, J., Pang, X., Yang, L., and Zheng, J. (2018). Structural style, formation of low angle normal fault and its controls on the evolution of Baiyun Rift, northern margin of the South China Sea. *Mar. Petroleum Geol.* 89, 687–700. doi:10.1016/j.marpetgeo.2017.11.001

Zhao, Z. Y., Zhao, J. H., Wang, H. J., Liao, J. D., and Liu, C. M. (2007). Distribution characteristics and applications of trace elements in Junggar Basin. *Nat. Gas. Explor. Dev.* 30, 30–33. (in Chinese with English abstract). doi:10.3969/j.issn.1673-3177.2007.02.007

Zhu, B., Yang, T., Wang, J., Chen, X., Pan, W., and Chen, Y. (2022). Multiple controls on the paleoenvironment of the early Cambrian black shale-chert in the northwest Tarim Basin, NW China: Trace element, iron speciation and Mo isotopic evidence. *Mar. Petroleum Geol.* 136, 105434. doi:10.1016/j.marpetgeo.2021.105434

Zhu, M. Z., Graham, S., Pang, X., and McHargue, T. (2010). Characteristics of migrating submarine canyons from the middle miocene to present: Implications for paleoceanographic circulation, northern South China sea. *Mar. Pet. Geol.* 27, 307–319. doi:10.1016/j.marpetgeo.2009.05.005

Zhu, W. L., and Mi, L. J. (2010). *Atlas of oil and gas basin, China Sea[M]*. Beijing: Petroleum Industry Press, 100–102. (in Chinese).